ELECTRON RECIRCULATION IN ELECTROSTATIC MULTICUSP SYSTEMS: I – CONFINEMENT AND LOSSES IN SIMPLE POWER LAW WELLS†

Robert W. Bussard

and

Katherine E. King

EMC2–0491–03

† This work performed under Contract No. MDA–972–90–C–0006 for the Defense Advanced Research Projects Agency, Defense Sciences Office.

EMC2® ENERGY/MATTER CONVERSION CORPORATION
9100 A Center Street, Manassas, VA 22110, (703) 330-7990

ELECTRON RECIRCULATION IN ELECTROSTATIC MULTICUSP SYSTEMS:

I - CONFINEMENT AND LOSSES IN SIMPLE POWER LAW WELLS

1. INTRODUCTION AND BACKGROUND

A large body of work over the past 35 years has been devoted to the study of cusp confinement of electrons, ions, and plasmas[1,2,3,4]. Nearly all of this has examined single particle electron (or ion) motion or the motion of particles in neutral plasmas within cusped magnetic systems, generally without internal electric potential fields. Furthermore, almost all of this work that concerned plasmas was limited to plasmas in local thermodynamic equilibrium (LTE); none applied to non-neutral systems. Nearly all were without internal E fields, and used cusp B fields, only; all particles studied were at constant (fixed) total kinetic energy throughout the system. And, almost all of the prior work focussed on biconic cusps[5] - which are uniquely unable to satisfy the configuration criteria necessary for effective electron confinement in Polywell^{tm}-type multicusp systems.

These are special polyhedral configurations[6,7] that allow formation of stable deep electrostatic potential wells in electron/ion mixtures by radial injection of energetic electrons into plasmas with net negative charge. Their spatial characteristics combined with the distribution of the internal E field arising from electron injection, and the induced predominantly-radial ion motion, result in long confinement times (due to many recirculation passes through the well before escape) for the electrons[8]. This is the *sine qua non* for minimum electron energy losses, under the conditions of large ion energy and core density achieved by the trapping of ion motion by the electron-driven internal potential.

Thus much, if not all, of the historical work on "cusp confinement" is simply not of relevance to the problem in Polywell^{tm} systems. Conclusions, perceptions, and "understanding" drawn from this body of work are thus often either irrelevant, valueless, or wrong. This is not to say that in itself

this work is of no value; rather, the systems it models and describes are so different in their determining physics that their conclusions can not generally be adjusted or modified to apply well to the Polywell^{tm} problem.

Conversely, some of the approaches used in generating these past studies have merit if used with care here. And, in any event, the models and analyses obtained for the Polywell^{tm} problem must reduce to those applicable to the simpler world of LTE, electrons-only and/or neutral plasmas, and cusps without E fields, when these reductions are put into the Polywell^{tm} models.

In this note the problem of electron motion, confinement and losses is analyzed in the non-LTE, electron-rich plasma system with anisotropic radial energy in both species, in multicusp Polywell^{tm} geometry. The bulk problem is treated as one-dimensional, with arbitrary spatial indices of radial B and E field variation. Bulk diamagnetic collective effects are modelled as they influence this 1-D spatial variation of B field, but electron entry into single cusp volumes includes elements of the geometric effects of the real 3-D configuration. Electron motions in mirror reflection regions are analyzed on the usual basis of conservation of magnetic moment of the electron at entry into the confining cusp. However, turning points of this motion are modified to account for the effects of diamagnetic currents on this process. Comparison with non-Polywell^{tm} models is made where useful and appropriate. Further details are given in the following sections.

II. CUSP MOTION: PROCESS DESCRIPTION AND TECHNICAL APPROACH

The general model of electron motion in the system is shown in Figures (1a) and (1b). Figure (1a) shows the model for non-diamagnetic behavior; Figure (1b) that for diamagnetic behavior of electron motion. In both figures the electrons are modelled as originating at the system center, at r = 0, moving through a non-adiabatic region to the "beta = 1" radius (r_b), thence to that radius (r_{ad}) at which adiabatic cusp reflection will occur, and finally to the outer radius, r = R, of the system.

Once they have reached a radial distance (r_x) at which their local gyromagnetic radius is sufficiently small that the total area of all of their gyro radius circles from each of the cusps is equal to the area of the spherical surface at that radius, they will enter one or another cusp in their outward motion. If r_b is less than this "transition radius" r_x the electrons move non-adiabatically without confinement, and enter each cusp at r_x, as shown in lines (a) of Figures (1a,b). No diamagnetic effects are yet effective at this point, as the gyro radius of electrons within $r_b < r_x$ is greater than the gyro radius at r_x, and coherent currents counter to the external B fields can not be generated and sustained.

Once r_b becomes greater than r_x the electrons inside r_b will "see" a lossy sphere with surface loss area (due to gyro radius area "holes") that is smaller than the sphere area at r_b, and they will be confined by internal reflection within this sphere. The average number of transits an electron will make within this sphere at r_b is just the ratio of the sphere area to the total loss area. As r_b grows larger (with increasing electron current input, and increasing central density - with requisite additional ions to maintain charge balance) this confinement grows larger, because the fractional hole loss area becomes smaller due to increasing B field strength at larger radial positions. This can be thought of as the confinement of a particle inside a perfectly-reflecting spherical shell perforated by holes - like the "wiffle ball" toy; and it is called "wiffle-ball" (WB) confinement. The average number of transits within r_b is defined here as G_{jwb}.

At some radius (r_{ad}) set by the mirror adiabaticity requirement that the local B field change only little over a local gyro radius, the electron is trapped in "mirror-reflection" (MR) oscillation within the cusp, as indicated in lines (b) of Figures (1a,b). Electron trapping in this (MR) mode is by the usual form of mirror reflection coefficient for motion in a single cusp mirror

system[1*]. This leads to a measure of the average number of transits G_{jmr} that an electron will make between $r_{ad} < r < R$ within this cusp mirror geometry.

In the non-diamagnetic model, as r_b is made larger still, so that it exceeds r_{ad}, the range available for the MR effect is reduced, as the electrons will now recirculate in the WB mode up to $r = r_b > r_{ad}$. This is shown in line (c) of Figure (1a). In the diamagnetic case, as r_b grows beyond r_x it begins to distort the externally-imposed polyhedral B field distribution to yield a configuration in which the field is compressed outwards by continuing exapnsion of the "beta = 1" surface (r_b). This results in the displacement of the adiabaticity radius (r_{ad}) to larger radii at a rate such that, with full diamagnetic currents, it will always fall outside the "beta = 1" radius. Thus r_{ad} recedes outwards as r_b exceeds r_x as shown in line (c) of Figure (1b).

Eventually (in the non-diamagnetic case) r_b reaches, or (in the diamagnetic case) r_b and r_{ad} reach a critical radius r_k at which further radial growth of r_b becomes unstable with respect to r. This is because the magnetic pressure balance criterion is satisfied for all radii beyond r_k, once it is reached at r_k. This radial position is that at which the electron (and ion) density begins to increase rapidly with $r > r_k$. Up to $r < r_k$ both ion and electron density fall approximately as $1/r^2$ from the core region at radius r_c with density n_c. Beyond r_k both ion and electron density increase rapidly, and the electron energy increases while the ion energy decreases as $r \rightarrow R$. Beyond r_k the electron density diverges markedly from the ion density in order to satisfy Poisson's equation and produce the desired negative potential well.

Once $r_b = r_k$ on this model, the behavior of the system "jumps" from r_k

---

[1*] The form for mirror reflection coefficient involves a term which is the square of the sine of the minimum trapping angle (relative to the B field) of electron motion in the B field at the trapping radius r_{ad}, for their escape at radius $r = R$. In the case of a system with electrons at constant energy and a B field varying as $\langle r \rangle^m$ this term varies as $\langle r_{ad} \rangle^m$. In the present case, the simultaneous radial variation of the E field reduces the reflection coefficient by virtue of the acceleration of electrons out of the system by the potential well gradient. If this E field is equal in magnitude to, and varies with the same functional form as the B field, no mirror trapping will be possible in the system. If the potential well is less deep than the electron injection energy, trapping is still possible, but with the reflection coefficient term reduced by a factor of about $(1 - a_q)$, where $a_q = e\phi_o/E_o$ is the ratio of well depth to injection energy. In the present note the mirror equations are all taken as for a system with $a_q \approx 0$, which overestimates the effect of mirror confinement. This issue is explored further in a forthcoming EMC2 technical note.

to R, where all further increase in system density buildup (by increasing electron and ion injection currents) is stopped at the levels relating drive current (I_e) and core density (n_c) attained at the $r_b = R$ condition. This is (obviously) because r_b can not physically become greater than R, even though mathematically this is possible, because the B field falls past $r > R$ and the electron loss area thus increases with increasing r. In short, the B field can not confine electrons at a density above that at which the surface electron energy density exceeds the energy density of the magnetic field system.

Therefore, when $r_b = R$ the core and bulk densities of electrons (and necessarily also of ions) are at their maximum values for the parameters defining the system (e.g. I_e, n_c, E_o, B_o, R). Further increase in electron drive current can not increase system density. Since fusion power output is proportional to the square of the core density, and since this is proportional to the surface density - and hence to the square of the B field - it is clear that increasing B field strength has a strong effect on system fusion power generation. On this simple argument, the fusion power will vary as the fourth power of the B field, just as for conventional magnetic confinement machines.

Initially, when electron injection is started, the only confining mechanism is mirror-reflection (MR) from the radius r_{ad} to R, over a number of transits G_{jmr}. As electron injection current is increased the WB mode develops when $r_b > r_x$, and the confinement parameter G_{jwb} grows progressively larger than unity. Particles between r_{ad} and r_b simply transit through this space. Since all particles that emerge from r_b (escaping the WB region) enter the MR region at $r > r_{ad}$, the total number of passes that an electron will make before loss is the product of those in each region.

In order to describe behavior of the "average" electron in the system, G_j in each region must be weighted by the number of particles in that region. For the $1/r^2$ density variation previously cited, this weighting is simply proportional to the region radial extent, running over $0 < r < r_b$ for the WB region and $r_b < r < R$ for the MR region. This simple weighting neglects the density increase in the region $r > r_k$, and thus underestimates the MR con-

tribution when $r_b < r_k$, and the WB contribution when $r_b > r_k$.

In order to analyze the complete behavior of the system, from initial injection of electron current to a final stable state of full density and full power operation, the dependent variable parameter needed is the average number of recirculations G_{jo} of the "average" electron in the system before its loss through r = R, and the variation of G_{jo} with system design and operating parameters. This is found by summing up the time spent in the MR mode with that spent in the WB mode and dividing this total system lifetime by the average time of transit of the average electron in one pass through the system. Thus, it is important to estimate this average transit time as correctly as possible if cusp losses are to be modelled with any degree of numerical correctness.

Unfortunately, this is not simple or straightforward in the real Polywell™ wells, because the electrons are not all unidirectional or monoenergetic. Rather, they have a distribution in both radial and transverse energy, and this governs their motion within the potential well. Furthermore, the potential well is not a simple monotonic power-law well, but has a central virtual anode in all systems of realistic interest (i.e. with large ion core density), as well as a "rollover" at the system boundary (this is not incorporated in the model used here; see Section VI, following).

The approach used was to divide the well into segments for the core, the central virtual anode, and the outer well region, taken here as monotonic, as shown in Figure (2). Then the transit time for the most energetic purely-radial electron was determined by integration of [dr/v(r)] in each region of the potential function. This resulted in an estimate of transit time t_{rtrn} in terms of the "injection time", $t_{in} = 2R/v_{in}$, defined as the time required for an electron to traverse the system diameter at its injection speed (i.e. in the absence of a potential well). A more detailed treatment of this problem is reported elsewhere[9].

To describe the transit time of the average electron in the initial electron input distribution required analysis of transit time variation across

this distribution, for typical potential well shapes[2*]. As used in the EKXL code this is a rectangular distribution in both total energy and transverse energy, being $E_{tot} = E_o \pm dE_{tot}$ and $E_{perp} = \pm dE_{perp}$. The energy spreads dE_{tot} and dE_{perp} may be chosen independently, subject only to the restriction that $dE_{perp} < dE_{tot}$. For these distributions it was found that the ratio of the transit time of the average electron to that of the most energetic purely-radial electron was approximately $[LN\langle t_{rin}\rangle]/[\langle t_{rin}\rangle - 1]$, where $\langle t_{rin}\rangle = (t_{rtrn}/t_{in})$. For almost all conditions of interest in the Polywell^{tm} system this gives the result that average transit times are 2-3 times the free-run injection time (t_{in}) previously defined. Figure (3) shows this ratio as a function of the core convergence ratio $\langle r_o\rangle$ and the virtual anode height parameter, taken from the more detailed analysis of this problem cited above[9].

III. ANALYTIC MODELS OF ELECTRON MOTION

Consider a simple monotonic potential well with magnetic field and electron kinetic energy variation as

$$B(r) = B_o\langle r\rangle^n \quad \text{and} \quad E(r) = E_o\langle r\rangle^n \qquad (1)$$

where $\langle r\rangle = (r/R)$.[3*] Now define the radius of transition (r_x) from uncorrelated to cusp-centered non-adiabatic motion by $4\pi(r_x)^2 = N\pi(r_L(r_x))^2$, where N is the (effective) number of point cusps in the system (in a system with all cusps identical, N is twice the number of full bi-polar magnetic axes) and r_L

[2*] This transit time for ions can be directly and easily calculated from the EKXL code. Not so for the electrons, however, as each element of the distribution must be followed through the distribution-dependent well at each time cycle. This makes it impossibly time-consuming on AT-level PCs, as the number of computations is so huge that it drastically increases the (already long) running time for each case. With larger CPU computing machines it is still an impractical computation.

[3*] The simple power-law form given for the B,E fields is not correct for real polyhedra with edge conductors forming the current carriers for the magnetic field coils. For example, the field varies inversely cubically within a truncated cube, but much less rapidly at radii approaching the equivalent spherical surface of the polyhedron. A more exact expression for the field is $B(r) = B_o\langle r\rangle^3[2/(1+\langle r\rangle^5)]$, which yields higher field strength within the system than is given by the simple power-law formula. The beneficial effect on electron confinement of this more realistic form is ignored in this present note.

is the "loss radius", defined as $r_L = k_L r_g$. Here k_L is a measure of the departure of gyro "hole" area losses from the strict single-gyro-radius (minimum) limit. The local gyro radius is

$$(r_g(r))^2 = 2E_o\langle r\rangle^m / r_e(B_o)^2\langle r\rangle^{2m} \quad \text{or} \quad \langle r_g\rangle^2 = 2w/r_e\langle r\rangle^m \tag{2}$$

where the term $w = E_o/(B_oR)^2$ is a parameter characterizing the system design, and $r_e = e^2/mc^2 = 2.818E\text{-}13$ cm is the classical radius of the electron. Note that $(2w/r_e)$ is the square of the ratio of electron gyro radius at the system boundary to the boundary radius, and is a measure of the "goodness" of mirror confinement; small w gives longer mirror lifetimes than large w. With these the transition radius in the unperturbed field is

$$\langle r_x\rangle = [Nw(k_L)^2/2r_e]^{1/(m+2)} \tag{3}$$

Similarly, the "adiabaticity radius" in the unperturbed field (r_{ado}) is defined, for an adiabaticity index[10] (Γ_a), as

$$[r_g(r_{ado})][dLN(B(r)/dr)]_{rado} = [r_g(r_{ado})][m/r_{ado}] = \Gamma_a < 1 \tag{4}$$

which yields

$$\langle r_{ado}\rangle = [2m^2w/r_e(\Gamma_a)^2]^{1/(m+2)} \tag{5}$$

Comparison of the criterion eq. (4) with computer simulation data[11,12] for electrons of fixed energy shows[10] that $\Gamma_a \approx (2/3)$ is a reasonable fit to the data for motion in the magnetic field configuration of a truncated cube.

As the electron density builds up within $r < r_b < r_x$ collective diamagnetic effects initially will be negligible, because the gyro radius at small r within this region is greater than the dimension r, itself. Increasing electron density will push r_b to larger radius and, when r_b approaches r_x, the diamagnetic currents due to internal electron gyro motion will begin to affect (reduce) the local B field amplitude. As r_b exceeds r_x and approaches r_{ad}, gyro currents become relatively stronger and more concentrated around the cusp axis, and this relative reduction in B field will increase.

This results in an increase in the gyro radius at the initial adiabaticity radius position (r_{ado}), such that the true adiabatic motion condition can no longer be satisfied at that radial position. The adiabaticity radius then moves further out into a region of larger B field. The net result is a progressive "pushing" of r_{ad} to larger radii, by r_b moving out with higher interior electron density. This pushing displacement can continue only to the critical density turnaround radius r_k, at which point $r_b = r_{ad} = r_k$ and r_b jumps to R, as discussed previously. This collective effect can be modelled crudely by a simple linear algorithm that scales the motion of r_{ad} from r_{ado} to r_k in proportion to the motion of r_b from r_x to r_k. The effective adiabaticity radius is then

$$\langle r_{ad} \rangle = \langle r_{ado} \rangle + k_a(\langle r_b \rangle - \langle r_x \rangle) \tag{6a}$$

where

$$k_a = (\langle r_k \rangle - \langle r_{ado} \rangle)/(\langle r_k \rangle - \langle r_x \rangle) \tag{6b}$$

The variable parameter of choice here is $\langle r_k \rangle$; all others are computed from system design or operating conditions. Thus k_a is not a universal constant, but is calculated for each set of $\langle r_x \rangle$ and $\langle r_{ado} \rangle$, each of which are fixed parameters for any given system. In a general analysis of particle density distributions, Krall[13] showed that the position of $\langle r_k \rangle$ depends on the the potential well shape. For typical well shapes of interest, $\langle r_k \rangle \approx 0.83$.

The "beta = 1" radius is the radial position at which magnetic pressure exactly balances electron kinetic pressure, $(n(r_b))(E(r_b)) = (B(r_b))^2/8\pi$. The variation of particle density with radius from the core density n_c at r_c is

$$n(r) = n_c(r_c/r)^2 \tag{7}$$

and defining the parameter $z = 8\pi n_c(r_c)^2$, yields the "beta = 1" radius as

$$\langle r_b \rangle = (zw)^{1/(m+2)} \tag{8}$$

Note that $(zr_c/6)$ is the total number of ions (or electrons) in the core.

The filling of the system so that r_b becomes greater than the transition radius r_x creates a WB confinement sphere with electron recirculation determined as $G_{jwb} = 4\pi(r_b)^2/N\pi(r_L)^2$. Using eqs. (2) and (8) gives this as

$$G_{jwb} = 2r_e z/N(k_L)^2 \tag{9}$$

Electrons leave this region $r > r_b$ relatively isotropically, and enter the MR region $r > r_{ad}$. Here they are recirculated with $G_{jmr} = 1/(1-R_{mr})$, where R_{mr} is taken here to be the usual[4*] mirror reflection coefficient[14]

$$R_{mr} \approx 1 - (N/4)(B(r_{ad})/B_o) \tag{10}$$

so that

$$G_{jmr} = 4/N\langle r_{ad}\rangle^m \tag{11a}$$

while $r_b < r_{ad}$ for the non-diamagnetic case, or for all r_b for the diamagnetic case, and

$$G_{jmr} = 4/N\langle r_b\rangle^m \tag{11b}$$

for $r_b > r_{ad}$, as previously discussed (this latter condition, eq. (11b), applies only in the non-diamagnetic case).

To determine the overall lifetime and mean number of passes made by an electron in the system it is necessary to find these parameters for each mode of confinement, and weight them by the fractional number of electrons participating in each mode.

The time an electron spends in the MR mode is just that during its transit time t_{mr} between r_b and R, multiplied by the number of MR mode recirculations G_{jmr}. Note that G_{jmr} is determined by motion over the radial interval $r_{ad} < r < R$ or $r_b < r < R$, while the transit time includes the non-reflec-

---

[4*] Also see discussion given in footnote 1*

tive region $r_b < r < r_{ad}$, if such exists. For $1/r^2$ variation of density, the number weighting function is just $(1-\langle r_b \rangle)$. Note that this underestimates the weighting because the density actually increases at $r > r_k$. The time spent in the WB mode t_{wb} is that while transiting the space $0 < r < r_b$, multiplied by the number of WB mode recirculations and the number of MR passes for each such recirculation. Its particle number weighting factor is simply $\langle r_b \rangle$; here correct as the density variation with radius is inverse-square in this region.

Determination of these transit times requires integration over the electron energy distribution in the potential well, for the several regions of the well that apply to each condition. Following the techniques outlined earlier for determination of total transit time across a virtual anode well (and detailed in an earlier note[9]) and making use of the potential functions for the virtual anode well shown in Figure (2), the separate transit times can be determined by piecewise integration for each region.

It is important to note that the definition of the relevant regions must also attend not only to the relative positions of $\langle r_x \rangle$, $\langle r_b \rangle$ and $\langle r_{ad} \rangle$ with respect to each other, but also with respect to the well minimum at $r = r_w$, as indicated in the figure. This is because it is not possible to integrate the potential distribution in closed form, and the integrals must be broken up on either side of r_w. Carrying this out results in the transit time formulae summarized in Figure (4). With these it is possible to write the recirculation ratios, G_j, as

$$G_{jo} = (4/N)(G_{jmro})(1-\langle r_b \rangle)(t_{mr}/t_{tot}) \qquad (12a)$$

for $r_b < r_x$, here entirely due to mirror-reflection within a multicusp system with effective number of cusps N, and

$$G_{jo} = G_{jmro}[(1-\langle r_b \rangle)(4/N)t_{mr} + (G_{jwb}-1)\langle r_b \rangle t_{wb}]/[t_{tot}] \qquad (12b)$$

for $r_b > r_x$. At this condition both MR and WB modes are acting; the first term is due to mirror effects, while the second is that due to wiffle-ball confinement. In these equations the term G_{jmro} has the meanings given below.

$$G_{jmro} = 1/\langle r_{ad}\rangle^m, \quad r_b < r_{ad}; \text{ and } G_{jmro} = 1/\langle r_b\rangle^m, \quad r_b > r_{ad} \qquad (12c)$$

These and all of their supporting equations are given in Figure (5), for convenient reference, for both magnetic and electric potential fields varying as a simple power law, $B,E \approx \langle r\rangle^m$. Using these formulae it is possible to calculate G_{jo} over a range of the system-defining parameters, (z) and (w). Note that w is defined by system external design criteria, while z is determined by internal conditions reached in the dense core during system operation. It is instructive to examine G_{jo} to see how the MR and WB contributions vary with these parameters.

Each of these can be calculated separately from their terms in the overall formulae for G_{jo}, from eqs. (12a,b,c). Calculations made for each of these separate terms are shown in Figures (6a,b) for an effective cusp number of N = 14,[5*] and B field spatial index of m = 3, for a typical set of system conditions with core convergence ratio of $\langle r_o\rangle$ = 1E-2, critical density radius of $\langle r_k\rangle$ = 0.83 and a loss radius factor of k_L = 2, for a potential well with virtual anode fractional height of η = 0.272. Note how G_{jmr} drops with increasing z (increasing core density) beyond the point where $r_b \geq r_x$. This is a result of the decrease in both MR mode time t_{mr} and in the weighting term $(1-\langle r_b\rangle)$, even before $\langle r_b\rangle$ reaches $\langle r_{ado}\rangle$. As $\langle r_b\rangle$ moves beyond $\langle r_{ado}\rangle$ the drop is even faster, as the diamagnetic effects of induced counter-currents in the electron flow become larger and "push" $\langle r_{ad}\rangle$ to larger radii.

The WB mode does not begin until $r_b > r_x$ and then rises rapidly with increasing z, t_{wb} and the weighting term $\langle r_b\rangle$. This is quite clearly seen in Fig. (6b), where the G_{jwb} curves fall rapidly to unity as (z/N) approaches a value of about 8E12/cm from above. The cutoff z value is determined directly from the equation for G_{jwb} by setting this equal to 1 (unity). Thus, for all

---

[5*] The actual effective number of cusps in a pure truncated cube system is only 9.6 for the MR mode operation, and 7.6 for the WB mode. These are determined by normalizing cusp losses for mirror reflection to B, and for WB losses to B^2, respectively, as described in an earlier note (ref.16).

values of $z < N(k_L)^2/2r_e$ the system will be operating solely in the MR mode. This has the inverse consequence that WB mode physics can be tested only if the experimental system is capable of being driven to a core density above this cutoff limit; $n_c(r_c)^2 > N(k_L)^2/16\pi r_e$.

Operation along a line of constant w above this point leads to a maximum G_{jwb} value at the boundary where $r_b = R$; beyond this point G_{jwb} no longer increases with greater input electron current. Also, at this point the electron (and ion) density within the system has reached its maximum value and all further density buildup is stopped, for here the system surface is already operating at an electron/magnetic beta of unity; more electrons can not be contained within this field. All of the early studies[15] of this concept were made along this line of maximum performance, at the condition $r = r_b$.

The sum of these two terms gives G_{jo} for the complete system. Figures (7a-e) show plots of this total G_{jo} for m = 3 power-law wells with a virtual anode, over a range of z and w, for several values of the gyro loss radius parameter k_L, and for convergence ratio and anode height taken as in the previous figures ($\langle r_o \rangle$ = 1E-2, η = 0.272). A series of calculations was made to test the effect of anode height on G_{jo}. These showed that the variation of G_{jo} with z and w is virtually independent of η for all $\eta > 0.01$. At very small $\eta \rightarrow 0$ the forms used for the transit time integrals begin to break down and give excessive transit times; for all realistic wells the dependence of G_{jo} on anode height is negligible for $0 < \eta < 0.3$.

It is useful to distinguish three regions of differing character on these figures. In the left hand region below (z/N) ≈ 1E12/cm the electron behavior is completely dominated by mirror-reflection effects. In this area the device is simply a multicusp mirror machine, operating with the usual MR features. In the right hand region above (z/N) ≈ 1E16/cm, electron behavior is completely dominated by collective mode wiffle-ball effects, and mirror phenomena have essentially vanished. Here and above (to z/N > 1E18/cm) lies the fusion reactor regime. This region is new and unfamiliar to the field of cusp plasma research; it forms the basis for the original Polywell™ concept

and the early studies[15] of its characteristics. In the middle region where 1E13 < (z/N) < 1E15/cm lies all of the physics of transition from MR to WB operation. Here is the region of greatest experimental and theoretical interest, for it is here that the physics features of the concept that allow transition to the reactor regime either will be found - or will not.

Several especially interesting features are evident from these figures. First, and of greatest importance, is that the overall electron recirculation ratio G_{jo} increases with increasing z, beyond some critical value of z. Elementary analysis, theory, and EKXL computer code runs all show that the core density n_c increases linearly with electron drive current above a core density of $n_c \approx$ 1E13-1E14/cm^3 if G_{jo} is held constant. Here, however, the value of G_{jo}, itself, is seen to increase with increasing electron current. Thus, once the critical z region is exceeded the core density will increase at a faster rate than the electron current. Taking the slope of the G_{jo} vs. z curve to be p (i.e. $G_{jo} \approx z^p$) it is easy to show that the core density will increase about as $n_c \approx (I_e)^{1/(1-p)}$ at this condition. The figures show that p $\approx$ (3/4) in this region, thus $n_c \approx (I_e)^4$ - a little extra electron drive current goes a long way - until G_{jo} stops when $r_b = R$, which marks the boundary limit for system operation, for any given value of the system design parameter w.

The second feature of importance is that the value of G_{jo} can drop with increasing z, from its initial low-z value, as operation leaves the MR mode - before WB mode confinement has taken any significant effect - subsequently increasing again as z becomes large, due to increasing dominance of WB mode operation. This drop is more pronounced and occupies a greater range of z as the loss radius factor is taken to be larger. This behavior constitutes a "gate" through which machine operation must be driven at startup. If the device is drive-current-limited, and if the current is insufficient (for the design values of w for the machine) to yield z values (e.g. core densities) beyond the gate, it will not operate above the much smaller z value to which the limited current can drive it. Here, in contrast to the positive slope of the WB regime, the slope of the G_{jo} vs. z curve is negative, say $G_{jo} \approx z^{-q}$, so that $n_c \approx (I_e)^{1/(1+q)}$. If q = (1/2), for example, then $n_c \approx (I_e)^{2/3}$ and a small

increase in core density can require a large increase in drive current. The actual state of affairs will depend upon the real values found for the gyro loss radius factor k_L, and for other dependent parameters that govern the operation and behavior of the electrons in the system.

It is very important to note the effects and characteristics anticipated for this device. In particular, a limited-current experiment that runs into the "gate" effect will demonstrate poorer electron (and ion) confinement with increasing current and core density. This is to be expected in this regime. Additional drive current past the gate point will show the opposite effect with core density increasing much more rapidly than electron current, once the G_{jo} vs. z slope has become positive.

Of course, the final use of the G_{jo} formalism outlined above, has been to "close" the EKXL code calculational scheme, to allow numerical estimation of these effects. The code now has been modified (as version 3.3) to include these phenomena, based on the power-law model with virtual anode used here. Until this was done, the variable G_{jo} was simply chosen as another arbitrary input parameter; now it is a dependent variable computed from system operating conditions at each time step so that all the relevant electron confinement physics is now working synergistically in the code[6*]. Further modifications of the electron cusp confinement model have been made to improve B and E field distributions. These are incorporated in an extended and further revised version (v.4.0) of EKXL, now in development, and are presented and discussed in a separate technical note, now in process.

Calculations using version 3.3 of the EKXL code have been made parametrically for a baseline case at high density ("reactor") conditions, and for several possible models of SCIF experimental systems and operations. Results of the SCIF computations are discussed in Section VI, following. Results of the reactor case studies are given here, in Figures (8a,b,c). Electron drive

---

[6*] This version of the code remains "open" in respect to self-regulation of the core size by competing collisional and angular momentum conservation mechanisms; it is planned to include these in a future code modification.

conditions, dimensions and other defining parameters are shown on the figures.

The basic case, shown in Figure (8a), was run with a virtual anode held at about 17 keV above the well bottom. Note the increase in core radius due to ion density buildup as the ions slow down towards this virtual anode core. In the core boundary region the ion density and the potential are both varying much faster than $1/r^2$. A parametric set of calculations was made to test this effect of anode height on core density and DD fusion power output. Results of these are given in Figure (8b), which shows that the competing effects of core broadening and ion slowing-down due to the anode change in such a way as to keep the core density and fusion output within a modest range of variation over a wide range of anode height.

Other studies were made for a 1000-fold variation of electron drive current, showing its effect on ion core density. Results of these, given in Figure (8c), show that the slope of the core density vs. current curve changes rapidly with increasing gun current, as described above from the G_{jo} curves of Figures (7a-e). The slope at I_e = 1000 A is approximately 4 (i.e. $n_c \approx (I_e)^4$) in good agreement with the effect of the G_{jo} vs. (z/N) slope of p = (3/4), as previously described.

IV. EFFECTIVE LOSS RADIUS; COMPARISON WITH CUSP MODELS

One principal area of concern in considering the multicusp Polywell^{tm} system, is how well the particles (especially electrons) will mirror-reflect; what will be the effective gyro loss radius in such a system? In an attempt to answer this question, considerable appeal has been made to prior models reported in the literature[1-5,16], and to single-particle orbit calculations[11] in this geometry. As noted earlier, much of this work is not directly applicable to the instant case, as it is monoenergetic, or uses single particles, has no potential well, or uses neutral plasmas in LTE, etc, etc. Still it is instructive to examine the question of effective loss radius in comparison with one of these models.

The Biconic "Spindle" Cusp Without E Field

Consider the system outlined by Grad[16], shown in Figure (9). This is a biconic cusp system, with no internal E fields, in which all particles are at constant energy. Beyond a critical radius r_x these are taken to be adiabatically trapped in flux shells outside r_x, while within r_x non-adiabatic motion is assumed, with isotropic emission into the polar point cusps at $r > r_x$. There are no collisions and no direct collective effects. Electrons in the cusp will move non-adiabatically out to larger r until they reach the adiabaticity radius r_{ad}. Here they still appear to the mirror region ($r > r_{ad}$) to be entering with isotropic distribution, as though from radius $r = r_x$. The equivalent value of k_L, as used previously (eqs. 1,3,9, et al), is then given by

$$(k_L)^2 = [r_g(r_x)]^2/[r_g(r_{ad})]^2 \qquad (13)$$

For the reference case with $B = B_o\langle r\rangle^m$ and E_o constant, the electron gyromagnetic radius is $[r_g(r)]^2 = 2E_o/r_e(B_o)^2(r/R)^{2m}$, and eq. (13) reduces to

$$(k_L)^2 = \langle r_{ado}\rangle^{2m}/\langle r_x\rangle^{2m} \qquad (14)$$

while for the general inertial-electrostatic Polywell^{tm}-type polyhedral point cusp system, with negative potential well index m, this becomes

$$(k_L)^2 = \langle r_{ado}\rangle^{m}/\langle r_x\rangle^{m} \qquad (15)$$

The adiabaticity radius is given by eq. (5) for the Polywell^{tm}, but has an exponent $1/(2m+2)$ for the reference case. Then eqs. (14) and (15) become

$$(k_L)^2 = [4m^2/N(\Gamma_a)^2]^{2m/(2m+2)} \qquad (16)$$

for the zero E-field biconic cusp, and

$$(k_L)^2 = [4m^2/N(\Gamma_a)^2]^{m/(m+2)} \qquad (17)$$

for the Polywell^{tm} polyhedral system.

The single biconic cusp has an equivalent number of poles equal to twice the number of polar axes, thus N = 4, while m = 3 for this field configuration (since $B \approx r^2 z$ around the origin). Taking $\Gamma_a = (2/3)$, as before, gives $(k_L)^2 = 9.54$ or $k_L = 3.09$ from eq. (16). The actual effective loss radius is one gyro radius larger than this because all particles whose guiding centers lie within r_g outside the radius $k_L r_g$ will pass inside $r \leq k_L r_g$, and thus can escape through this loss channel. The effective electron loss radius is then $k_{Lo} = k_L + 1 = 4.09$, in reasonable agreement with the values cited by Grad[17].

Losses through the the equatorial ring (line) cusp in the biconic configuration have been asserted[17] as limited to escape through an "escape width" δ_{eq} given by geometric arguments of equality of magnetic flux area from the polar point cusps through the equatorial ring; thus $(\delta_{eq}/r_g) = (r_g/R)$, where r_g is taken as the gyro radius at the system surface (r = R). In fact, for the reason cited above, particles within a guiding center one r_g distant can pass through this escape width and be lost. Thus the effective loss-escape area is $A_{eq} = 2\pi R[\delta_{eq} + k_{Lo} r_g(R)]$, which is dominated by the gyro loss radius, as discussed by Leung, et al.[18] This is to be compared with escape through the two point cusps with area $A_{pt} = 2\pi[r_g(R)]^2[k_{Lo}]^2$.

For operation at high-field, high-density conditions (as for useful reactor level systems) $r_g \ll R$, thus $\delta_{eq} \ll r_g$ and the ratio of equatorial to polar point cusp escape areas $A_{eq}/A_{pt} = R/[k_{Lo} r_g(R)]$ can become very large. For the biconic "spindle" cusp as a multipole system with equivalent number of point cusps N = 4, the effective loss radius factor for equatorial losses is then found to be simply $k_{Leq} = \{k_{Lpt} R/[r_g(R)]\}^{0.5}$, where $k_{Lpt} = k_{Lo}$ above.

Polyhedral Multicusp Systems With E Fields

For the polyhedral negative-potential-well system, similar arguments give $k_L = 2.03$, $k_{Lo} = 3.03$ for m = 3, with $N = N_e = 7.6$ (B^2-effective cusps in truncated cube geometry[19,20]), $\Gamma_a = (2/3)$, from eq. (17). If the cusp system had a true effective number of cusps of N = 14 (i.e. if all cusps were identical), eq. (17) would yield $k_L = 1.69$, and $k_{Lo} = 2.69$.

It is also of interest to determine how k_L, k_{Lo} vary with the number of cusps in Polywell^{tm}-type polyhedral systems. For the simplest polyhedra, the pole number and spatial exponent are related roughly as given below

Number of poles	(N)	8	14	26	50
Spatial exponent	(m)	2	3	4	5

so that the pole number and spatial exponent can be approximated by

$$m^2 \approx N/1.7 \qquad (18)$$

With this form, eq. (17) reduces to $(k_L)^2 = [4/1.7(\Gamma_a)^2]^{m/(m+2)}$ which gives $k_L = 1.65$, $k_{Lo} = 2.65$ for $m = 3$.

The limiting condition for very large N can be found by examination of the B field variation with radial position in the case of high-order multipole fields. These were analyzed in a previous note[21] which showed this to be

$$B(\sigma) = (B_o/\sigma^3)EXP(-\sigma) \qquad (19a)$$

where $\sigma = z/r_p$ is the ratio of distance in from the outer boundary, $z = r-R$, to the interpolar spacing $r_p = 2R/N^{0.5}$. Reducing terms this becomes

$$B(r)/B_o = [8/N^{3/2}(1-\langle r\rangle)^3]EXP[-N^{0.5}(1-\langle r\rangle)/2] \qquad (19b)$$

Setting this equal to $\langle r\rangle^{m_e}$ defines the equivalent exponent m_e in terms of N and $\langle r\rangle$. This can be found by taking logarithms of both sides and letting N approach ∞. The dominant term remaining gives this exponent approximately as

$$(m_e)^2 \approx (N/4)[(1-\langle r\rangle)/(LN(1/\langle r\rangle)]^2 \qquad (20)$$

as compared with eq. (18). With this the effective loss radius factor becomes

$$k_L \approx (1-\langle r\rangle)/\Gamma_a LN(1/\langle r\rangle) \qquad (21)$$

as the limiting case when $N,m \rightarrow \infty$, for which $\sigma \approx 0$. This results in mirror reflection only in the region $r \approx R$ ($\langle r \rangle \rightarrow 1$), at which condition eq. (21) reduces to $k_L \approx 1/\Gamma_a = 1.5$, and $k_{Lo} \approx 2.5$.

Thus the loss radius factor for polyhedral systems seems to be in the range of $2 < k_{Lo} < 3$; i.e. electron losses in the WB mode will proceed as though leaking out through holes with an "escape" radius 2-3 times that of the local gyro radius at the wiffle ball surface at $r = r_b$. The overall electron recirculation ratio, $G_j = G_{jo}$, for these cases is as shown in Figs. (6b,c). Note that k_{Lo} values in this range begin to yield the gate effect for devices operating with design parameter w-values in the range expected for reactor level operation ($1E-3 > w > 1E-5$ keV/(kGcm)^2).

V. COMPARISON WITH EXPERIMENT: THE CURRENT SCIF DEVICE

The EKXL code v.3.3 using the simplified power-law formalism outlined above was used to calculate a number of approximations to SCIF cases, in order to assess the viability of the current SCIF device to test the Polywell^{tm} concept for its critical physics. Code runs were made for several different models of operation modes proposed for the experiments. These were:

(a) Electron injection of 75 A (maximum possible) at full radius (R = 92 cm), with a central B field of $B_o = 3.1$ kG in the circular coils located on the square faces, but with the ion source at 61 cm radius. Ions were created by electron cyclotron resonance heating (ECRH) at the 875 G magnetic field at that point. The electron energy here was 6.6 kV, following the simple power law form used earlier, from injection with 22.5 kV at r = R = 92 cm. This outer radius was used to fix the value of the parameter w at that for maximum radius, voltage and field; w = 2.76E-4 (keV/(kGcm)^2). This parameter has a controlling effect on electron losses and thus on G_j. This set of conditions matches those initially planned for SCIF experiments, and is a reasonably realistic mockup within limitations of the EKXL code.

(b) Operation of the system at the small (ECRH-set) 61 cm radius, only, but with full 22.5 kV (maximum currently possible) electron injection energy, at 75 A current. This case mocks up the hypothetical prospect that the potential may be kept relatively flat from the outer radius at 92 cm to the ECRH ion source radius at 61 cm, with only partial electron neutralization by background ions in this region. The B field at this 61 cm surface is B = 875 G and the w value was taken as that for this value of B_o in the small system with full electron injection voltage. This was a case to test the effect of an assumed external flat potential region. Its value of w is least favorable to the attainment of high core density; w = 7.90E-3 $(keV/(kGcm)^2)$.

(c) Operation with the surface B field reduced to the ECRH 875 G, so that the ion source is at the outer boundary of the device, and use of 22.5 kV for electron injection energy, again with 75 A electron current. This is the ECRH small-radius case (a) with B field reduced to move the ion source radius to the outer boundary of the device. The w value for this case is that for the full radius of the device, with full drive voltage E_o but less magnetic field B_o than that actually available; w = 3.47E-3 $(keV/(kGcm)^2)$. This case was to test the effect of using the available ECRH ion supply at the full radius of the existing SCIF experimental machine.

(d) System operation with the full B field and maximum electron drive current (75 A) and voltage (22.5 kV) at the outer 92 cm radius, with ion injection at this boundary, rather than supplied at the lesser field and radius planned for use of the ECRH scheme. The w value here is that for the full system, as in case (a); w = 2.77E-4 $(keV/(kGcm)^2)$. This case tested operation at the best conditions for confinement and for high ion energy that could be hoped for experiments with the SCIF device with its current electron drive capability (however, note that the current SCIF system has no provision for ion injection at r = R with the full B field).

These conditions are summarized in Table 1, following, for reference.

TABLE 1

SCIF MODELS ASSUMED FOR EKXL CALCULATIONS USING ELECTRON MULTICUSP MODEL

CASE	RADIUS OF IONS	RADIUS OF ELECTRONS	ELECTRON ENERGY AT WELL EDGE	ELECTRON ENERGY AT INJECTION	B FIELD AT WELL EDGE	B FIELD AT FOR W	W, kV/(kGcm)^2 $E_o/(B_oR)^2$	REMARKS
(a)	61 cm	92 cm	6.8 kV	22.5 kV	0.88 kG	3.1 kG	2.8E-4	SCIF experiment case
(b)	61 cm	61 cm	22.5 kV	22.5 kV	0.88 kG	0.88 kG	7.9E-3	Flat outer potential
(c)	92 cm	92 cm	22.5 kV	22.5 kV	0.88 kG	0.88 kG	3.5E-3	Reduced surface B field
(d)	92 cm	92 cm	22.5 kV	22.5 kV	3.1 kG	3.1 kG	2.8E-4	Ions at r=R, w/full B,E

EKXL code calculations were made for these cases for two different values of the loss radius factor k_L, for ion injection energies taken always such that the core radius was r_c = 1 cm. These energies are expected from the ECRH ionization process planned for the experiments. All cases were run with an equivalent effective number of cusps of N = 14, and a specified virtual anode height of η = 0.11, except for case (a) which used η = 0.03. The maximum core densities n_c and recirculation ratios G_{jo} obtained from these calculations are summarized in Table 2, below.

TABLE 2

RESULTS OF EKXL v.3.3 CALCULATIONS FOR SCIF CASES OF TABLE 1

SCIF CASE	LOSS RATIO k_L	RECIRCULATION RATIO, G_{jo}	CORE DENSITY n_c, 1/cm^3
(a)	1	230	2.02E13
	3	42	3.70E12
(b)	1	6	1.77E11
	3	6	1.77E11
(c)	1	10	3.21E11
	3	10	3.21E11
(d)	1	52	1.92E12
	3	52	1.92E12

The full system radius applied to both ions and electrons in the runs for cases (c,d). Cases (a,b) were run with both species at 61 cm, even though the electrons were injected at 92 cm, since these cases operated with ion

input at the small radius (61 cm). Solutions obtained in these runs may be superposed with electron distributions found from full radius cases, since both species use the simple power law (m = 3) variation. By these means EKXL code results can be used to estimate SCIF experiment conditions, even though the code can not be used directly with the dual radius injection constraint.

Results for steady-state potential and density distributions are shown in Figures (10) and (11) from EKXL code runs for cases (a,d) with $k_L = 1$. From these figures and the data available from the code output for the other cases, it is possible to determine the relation between electron recirculation ratio G_{jo} and ion/electron core density n_c and radius r_c, as each test device starts up and rises to steady operation. This is plotted on the lines of constant w in Figures (12a,b), which show the range of these variations for each of the SCIF cases listed above, on the general graphs of G_{jo} vs. z/N for various w values (from Figures 7a,c), for two values of the loss radius factor k_L.

The important point to note here is that the regions in which the SCIF test cases are computed as able to operate (on the simplified model used here) are all at the left hand side of the figures, where electron confinement (and device) behavior is dominated by mirror-reflection physics. The only case that can reach the collective wiffle-ball mode region is that of case (a) at $k_L = 1$, with small effective w, but with the small radius system. This is the only case that succeeded in getting past the "gate". For this case the parameter $z/N \approx 4E13/cm$, just into the lower boundary of the WB mode region.

When the experiments are actually run, if the loss radius factor is found to be small (e.g. $k_L \approx 1$) then the WB effect will have begun by the time this z value is attained, and some degree of testing of the WB physics will be possible. On the other hand, if k_L is found to be as large as 3, for example, the WB region will not be reached in this example case. The other small w SCIF system (case d) falls about an order of magnitude lower in z/N, even with $k_L = 1$, at $z/N \approx 3E12/cm$; again not quite into the WB mode. And all of the other cases yield even lesser results.

Based on these computations, test of the physics relevant to the WB confinement concept requires operation of the experimental device at considerably larger electron drive currents or at higher B fields (or both) than those used in the calculations. If the electron injection voltage could be reduced while increasing current output, keeping power constant, the value of w could be reduced. This would result in an increase in G_{jo} and an extension of the experimental regime further into the WB mode phenomenology space. Of course, another means to achieve this desideratum is to add electron guns, and raise their voltage to increase their current output (since $I \approx V^{3/2}$ in the existing guns), which requires larger power supplies to drive the system. Without some means of increasing drive conditions and decreasing w, the model presented here suggests that the current SCIF device can test the collective physics that forms the basis of the Polywell^{tm} concept only marginally, if at all. However, note that the $\langle r \rangle^m$ power law model used here is certain to underestimate electron confinement, and that more correct models will yield better performance. This is discussed briefly in the following section.

VI. ELECTRON MULTICUSP MODEL; LIMITATIONS AND IMPROVEMENTS

The simple model presented above for electron trapping and losses in the complex Polywell^{tm} multicusp magnetic field system with internal electrostatic potential well, is based principally on the spatial variation of both B and E fields assumed as following a simple power law of the form $B,E \approx \langle r \rangle^m$. In actual fact, the magnetic field distribution within the volume bounded by a polyhedral coil system that fits the Polywell^{tm} criteria is not so simple. In a similar vein, the linear displacement of the adiabaticity radius r_{ad} is an overly simple approximation to the somewhat complex changes in internal B field distribution caused by the generation of diamagnetic currents and their consequent collective effects on the system. And, of course, the treatment of MR mode confinement here is too simple, in that the deleterious effects of non-zero potential well depth are not accounted for in the elementary formulae used to describe MR mode electron recirculation. In fact, magnetic mirror reflective confinement can be reduced severely if well depths are allowed to become too large during startup. These issues are examined next, below.

Magnetic Field and Electric Potential Distributions

Studies[22,23,24] have shown that the field variation asymptotically approaches the simple power law form only as the radius becomes smaller (approaching the origin) within the system. At radii beyond about $\langle r \rangle = 0.5$, the field modulus exhibits a "bumpiness", and its variation in any plane section through the center of the system and one of the edge midpoints always shows a "rollover" as the edge of the system is approached. Figure (13) shows an example of this sort of variation with radial position.

The effect of this realistic departure from the power law assumed in the model, above, is beneficial to electron confinement because it gives larger B fields at deeper radii than does the simple power law (for the same face cusp central field strength). The simple model is thus likely to yield results that are conservative (or pessimistic), because of its underestimate of the strength and effects of the real magnetic fields in the system. This can be rectified by employing an improved description of the B field, which better mocks up the actual variation within the polyhedron. Limiting this, as before, to radial-only dependence (1-D can be analyzed in closed form; 2-D can not) it is found that the edge effects can be accounted for in an approximate way by use of the form

$$B(r) = B_o\langle r \rangle^m f_o(r) = B_o\langle r \rangle^m [2/(1+\langle r \rangle^{m+2}] \qquad (22)$$

It is obvious from this that the field strength well within the system will be twice that previously used, for the same value of cusp central-axis maximum field strength, B_o. As a result, the electron gyro radii at these inner radial positions will be roughly one-half of those previously estimated, with concomitant improvement in electron confinement.

This simple formula has the advantage that it will still yield analytic solutions for most (but not all) of the parameters which characterize the system and are used in the solution methods employed in the model described here (e.g. the specific dimensionless radii $\langle r_{ad} \rangle$, $\langle r_b \rangle$, $\langle r_x \rangle$, and the separ-

ate mode recirculation ratio terms G_{jmr} and G_{jwb}). Unfortunately, the transit time integrals can not be obtained in useful closed forms with this more realistic potential variation. However, since the transit time segments used in the calculation of the electron recirculation are divided by the total transit time in the expression for the overall system G_{jo} ratio, the effect of integral departures from exact behavior are minimal for this factor, thus these times can be taken in the forms used previously, without serious error. Further analysis of electron confinement is underway using this modified formalism. A discussion of these analyses and presentation of their results is given in a forthcoming technical note.

Diamagnetic Effects

A second area in which system modelling might be improved is that of collective effects giving rise to diamagnetic expansion of the B field and the consequent shift in position of the adiabaticity radius $\langle r_{ad} \rangle$. Although better than the use of the non-diamagnetic approximation, the linear formula of eq. (6a) is a relatively poor approximation to the displacement of the adiabaticity radius by real diamagnetic current effects. These tend to act in an energy-conservative fashion, such that the volume integral of the magnetic field energy remains fixed as the field is distorted by the increasing internal electron density (which is, itself, supported by the induced ion density) causing expansion of the beta = 1 surface $\langle r_b \rangle$. Beyond the transition radius $\langle r_x \rangle$, increasing $\langle r_b \rangle$ will tend to push the excluded external B field into the volume remaining between $r_b < r < R$. This "pushing" will cause the field to pile up outside r_b as this expands, giving a region of steep field gradient, followed by one with a smaller gradient than before.

If a simple power law form is assumed for the B field outside r_b, it is possible to integrate B over this space and determine an equivalent exponent (m) that conserves B field energy, for each position of r_b. Or, with greater complexity, the modified power law described above can be invoked and used to find the equivalent exponent for this form of the B field spatial variation. Neither approach is correct, in that both will yield a B field mean exponent that decreases as the central beta = 1 region expands towards the system outer

boundary. In actuality, the B field compression outside of r_b will give a larger spatial exponential index within this region, while the decreased field gradient at greater radii will yield a smaller value of equivalent m. In this situation the adiabaticity radius will move slowly inward, or stay relatively fixed in position, until r_b comes within a few gyro radii of r_{ado}. At this point the increasing gradient in local B field will cause r_{ad} to recede outward almost directly with r_b.

The net result is a complex motion in which the shift of r_{ad} is less unfavorable (to electron confinement) than by the linear model assumed above, so that the MR mode will hold up somewhat longer and larger values of G_{jmr} will characterize the analysis than those obtained from the model herein. The result of all this will be an increase in the estimated performance, in that larger values of core density can be attained for given drive current than from the simple model here. However, the effect is expected to be slight, since the change in critical radii (e.g. $\langle r_b \rangle$, $\langle r_x \rangle$) will only depend on the one-fifth root of the change in the B field. The value of developing and including such modifications for diamagnetic effects is not clear in light of the various approximations already employed in this analysis.

Multicusp Mirror Reflection and System Startup

Startup of the system is a complex problem. The bulk electron and ion core densities must be built up through the MR mode to levels sufficient to operate in the WB mode thereafter. In the MR mode, electron confinement is due to cusp mirror trapping with eventual reflection by the rapidly-increasing (with r) B field. The ratio of electron gyro radius to radial position drops steadily with increasing r, as $r^{(m+2)/2}$, even in the least favorable case, when the E and B fields both vary as $\langle r \rangle^m$.

Initially the well has no depth; it is flat across the system. Electrons injected at low current and low density make little effect until they reach a value of the order of 1E5 - 1E6/cm^3, in systems of R = 100 cm, or so. At this level of bulk density the well will begin to be visible, at a depth of 0.1-1.0 keV, without ions. The addition of ions to the system will create a

more tightly focussed distribution but even this will not result in significant well depth at these electron density levels. Typically, Poisson's equation gives $E_w \approx 3E5[n]$ keV for [n] as mean density per cm^3, in a 100 cm radius electro-kinetic well of the type here.

As [n] exceeds this range the well begins to deepen. This causes the MR confinement to degrade because of the appearance of an accelerating electric field within the confining magnetic field structure, coupled with conservation of electron magnetic moment in this field. The effect is due to the extraction of the energy needed to increase the transverse kinetic energy of electrons in cusp-trapped gyro motion, from their energy gain in the potential field by radial outward motion of the cusp electrons, rather than from their radial kinetic energy at the trapping point.

The relevant correction factor to multiply the formula for the electron recirculation ratio G_{jmr} can be shown to be $[(1-a_q) + (a_q\langle r_{ad}\rangle^m)]$ for a system in which both the E and B fields vary as $\langle r\rangle^m$. Here the term $(1-a_q)$ is the ratio of the difference between the well depth and the electron injection energy to the injection energy; it is the fractional "unused" potential in the system; $a_q = e\Phi_o/E_o$, where $e\Phi_o$ is the potential well depth at its point of maximum amplitude, and E_o is the injection energy of the electrons that are driving the system. It is evident that operation at full well depth, which gives $a_q = 1$, will yield $G_{jmr} = 0$, and a well incapable of any electron confinement by mirror reflection processes, at all.

Thus, operation of the system by (a) control of electron current and voltage, and of ion current into the system, requires the following steps:

1a. Start with a small electron current, raise the density to the initial significant range (ca. $1E6/cm^3$). This should produce a shallow well, but one capable of confining ions at some modest fraction of the electron injection energy.

2a. Add ions thereafter to neutralize further well depth growth, as electron current is increased to larger values. This should yield increasing ion core density, following along with the increasing electron density.

3a. This process should be continued until the ion and electron core density has reached a value well into the WB range (e.g. to z/N > 1E14/cm). Use of virtual anode (height) control (VAC) of ion input rate is required to achieve this electron and ion density increase in a well-controlled manner.

4a. Then reduce the allowed VAC height, reducing ion input, to deepen the well while maintaining the high ion core density needed to stay in the WB regime beyond the gate in the G_{jo} vs. z/N parameter space.

5a. Once high core density has been achieved with reasonable well depth, the device can be driven harder (as a WB machine) with more electron input to reach desired operating conditions beyond those of the startup phase.

An alternate method of startup is to (b) control injection voltage and current and use controlled input of background neutral gas as the source of initial ions in the system core, following the sequence:

1b. Raise background neutral gas to high density - well into the WB region. Typically this is the order of 1E15-1E16/cm^3. After ionization and heating this density will drop by at least an order of magnitude; it must still remain in the WB regime to be effective.

2b. Drive electron current at modest voltage into the system to produce a small negative well and strong centrally-peaked ionization of background gas. Even though the ions are cold, this constitutes the core ion source needed for bootstrap startup. Cold electrons are driven out by the negative potential well.

3b. When the core ion density exceeds the z/N needed for WB regime operation by at least ten-fold, then increase the electron voltage to the desired value of w for system operation. This will yield a deeper well and begin to "heat" the cold central ions, some of which will begin to Maxwellianize. Be careful to add ions slowly here, so as to avoid inhibiting the increase of well depth due to increasing electron voltage.

4b. Then raise electron current, but now with ion edge input under VAC to continue partial neutralization until full required core density is reached with high energy ions. From this point the device can be run as a WB machine to any higher desired operating point.

In both approaches, the objective is to operate the device initially as an electron-trapping multicusp mirror machine without significant degradation of MR cusp reflection by the negative gradient of a deep potential well. Then to build up ion density - albeit at low energy - by continued injection of both species while maintaining well depth sufficiently small to avoid degradation of MR mode confinement. By this means to build up ion density to the WB range of z/N, where the slope of the G_{jo} vs. (z/N) curve has become large and positive. Then, finally, to transition to higher z/N and higher w values by increasing electron voltage and current (and associated increased ion supply) for straight WB operation at the desired steady operating parameters.

Here, just as in classical mirrors, startup is the problem. In the first scenario, startup MR degradation is limited by direct control of well shape by VAC of ion input to constrain the system to shallow wells. In the second one, this is accomplished by creation of a shallow well with a high density cold plasma/ion core in the body of the system, where cold electrons are expelled and cold ions are trapped.

In either case the electron MR confinement process can be analyzed by use of modified models for description of trapping at the adiabaticity radius, and subsequent MR mode operation, as described above. All of the relevant critical radii depend on the key well-depth parameter (α_q), as does the MR ratio G_{jmr}, but the WB mode electron recirculation G_{jwb} does not. The system performance equations can be cast into a form in which the controlling cusp reflection is made to have a functional dependence on the system operating state through connection with the VAC parameter, thus allowing feedback control of well depth to be used to optimize electron confinement. Finally, it may prove possible to create a system in which the E field and B field do not follow the same spatial form. Although the means to achieve this are not yet evident, this sort of behavior can be modelled to test its effect on electron confinement in the MR mode. It is hoped to include these more detailed effects, as well as others discussed above, in further analysis of electron cusp motion and confinement phenomenology, for inclusion in the next version of the EKXL code, now in development.

REFERENCES

1. I. Spalding, "Cusp Containment," in Advances in Plasma Physics, Vol. x, 1971, pp. 79-123

2. D.G. Blondin and T.J. Dolan, "Equilibrium plasma conditions in electrostatically plugged cusps and mirrors," Jour. Appl. Phys. Vol. 47, No. 7, July 1976, pp. 2903-2906

3. P.J. Catto and J.B. Taylor, "Electrostatic Enhancement of Mirror Confinement," Nuclear Fusion, Vol. 24, No. 7, (1984) pp. 229-233

4. O.A. Lavrent'ev, "Electrostatic and Electromagnetic High-Temperature Plasma Traps," Conference Proceedings, *Electrostatic and Electromagnetic Confinement of Plasmas and the Phenomenology of Relativistic Electron Beams*, Ann. N.Y. Acad. of Sci., Vol. 251, 1975, pp. 152-178

5. J. Berkowitz, et al, "Cusped Geometries," *Proceedings of the Second International Conference on the Peaceful Uses of Atomic Energy, Geneva, 1958*, United Nations, Geneva, Vol. 31, 1958, pp.171-176

6. R.W. Bussard, "Method and Apparatus For Controlling Charged Particles," U.S. Patent Number 4,826,626, May 2, 1989, assigned to Energy/Matter Conversion Corporation (EMC2)

7. R.W. Bussard, G.P. Jellison and G.E. McClellan, "Preliminary Research Studies of a New Method for Control of Charged Particle Interactions," Pacific-Sierra Research Corp. Report No. PSR-1899, 30 Nov. 1988, Final Report under Contract No. DNA001-87-C-0052, Defense Nuclear Agency, Sect. 1

8. R.W. Bussard, "Some Physics Considerations of Magnetic Inertial-Electrostatic Confinement: A New Concept for Spherical Converging-Flow Fusion," Fusion Technology, Vol. 19, No. 2, March 1991, pp. 273-293, Sect. III-C

9. R.W. Bussard and K.E. King, "Electron Transit Time in Central Virtual Anode Wells," Energy/Matter Conversion Corp., internal Technical Note, EMC2-0291-03, Feb. 1991

10. R.W. Bussard, "Comparison of Models and Computer Simulations of Single Particle Electron Confinement in Multicusp Polywell™ Systems," Energy/Matter Conversion Corp., internal Technical Note, EMC2-0391-02, Mar.1991, Sect. III

11. K. Maffei, "Single Particle Electron Confinement Study," Directed Technologies Inc., DTI internal technical note, Aug. 2, 1990

12. S.K. Wong, et al, "Statistical Study of Single Particle Confinement in a Cusped Magnetic Field," Energy/Matter Conversion Corp., internal Technical Note, EMC2-0491-02, Apr. 1991.

13. N.A. Krall, "Density Profiles in the Polywell™/SCIF Device," Krall Associates, internal Technical Report, KA-90-51, Dec. 1990

14. S. Glasstone and R. Lovberg, *Controlled Thermonuclear Reactions*, D. Van Nostrand Co., Inc., Princeton, NJ, 1960, Chap. 9, Sects. 9.5-9.7, 23, 24

15. Op cit ref. 8, Sect. VI-A

16. H. Grad, "Containment in Cusped Plasma Systems," in *Progress in Nuclear Energy*, Series XI, *Plasma Physics and Thermonuclear Research*, Vol. 2, ed. by C.L. Longmire, J.L. Tuck and W.B. Thompson, Pergamon Press, 1963, pp. 189-200

17. Op cit ref. 14, Sect. 3, "Containment Formulas"

18. K.N. Leung, N. Hershkowitz and K.R. MacKenzie, "Plasma Confinement by Localized Cusps," Phys. Fluids, Vol. 19, 1976, pp. 1045-

19. R.W. Bussard, "Geometric Gyro Radius Losses in the SCIF Experimental Device," Energy/Matter Conversion Corp., internal Technical Note, EMC2-1290-02

20. R.W. Bussard, "Effective Number of Cusps for Mirror Reflection and Wiffle-Ball Confinement in Polywell™/SCIF Systems," Energy/Matter Conversion Corp., internal Technical Note, EMC2-0491-04

21. R.W. Bussard, "Approximate Variation of High Order Multipole Fields," Energy/Matter Conversion Corp., internal Technical Note, EMC2-0890-02

22. Op cit ref. 7, Appendix C, p. 189, Figure 2-1, "Magnetic field along square face axis; truncated cube"

23. N.A. Krall, "The Polywell™, A Spherically Convergent Ion Focus Concept," Krall Associates, internal Technical Report, KA-90-45, Feb. 1991, to be published in *Fusion Technology* (1991)

24. S.K. Wong, "Structure of the Polywell™ Magnetic Fields," Energy/Matter Conversion Corporation, internal Technical Report, EMC2-0391-04, Mar. 1991

LIST OF FIGURES

FIG. 1(a) NON-DIAMAGNETIC MODEL FOR ELECTRON CONFINEMENT IN MULTICUSP POLYWELL^{tm} SYSTEMS

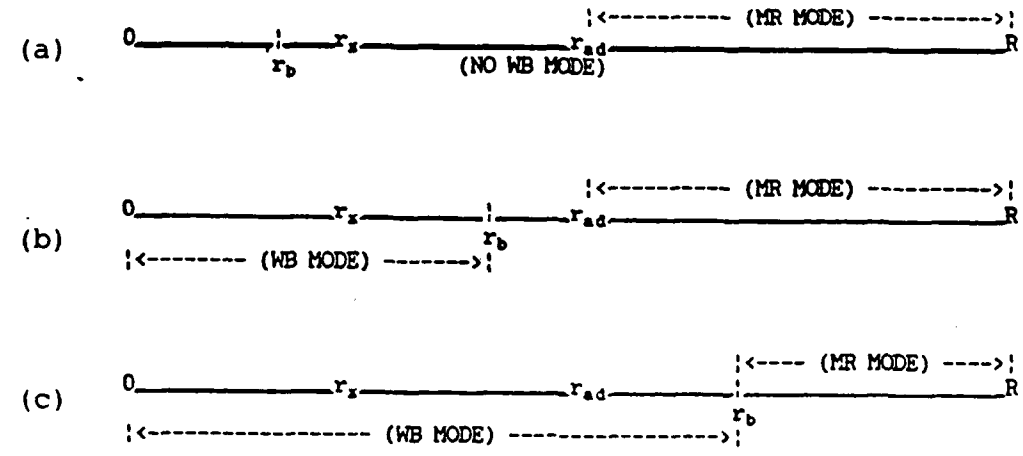

FIG. 1(b) DIAMAGNETIC MODEL FOR ELECTRON CONFINEMENT IN MULTICUSP POLYWELL^{tm} SYSTEMS

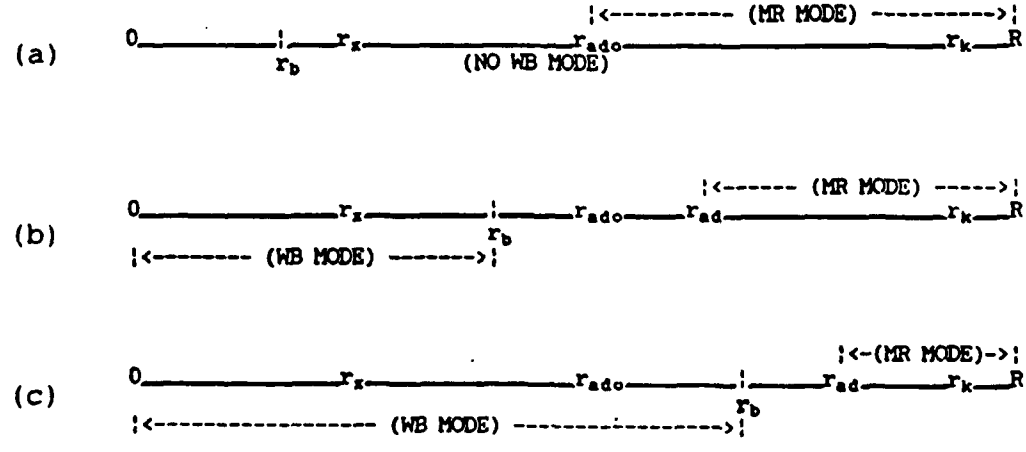

1. Schematic outline of system behavior and parameters. (a) Non-diamagnetic model; (b) Diamagnetic model. Lines (a)->(b)->(c) on each figure denote increasing electron drive and ion supply currents

EMC2

Figure 2 General potential distribution in well with central virtual anode, $E_{ao} = (E_o - e\Phi_{ao})$, with potential maximum (well minimum) at turning–point radius, r_w

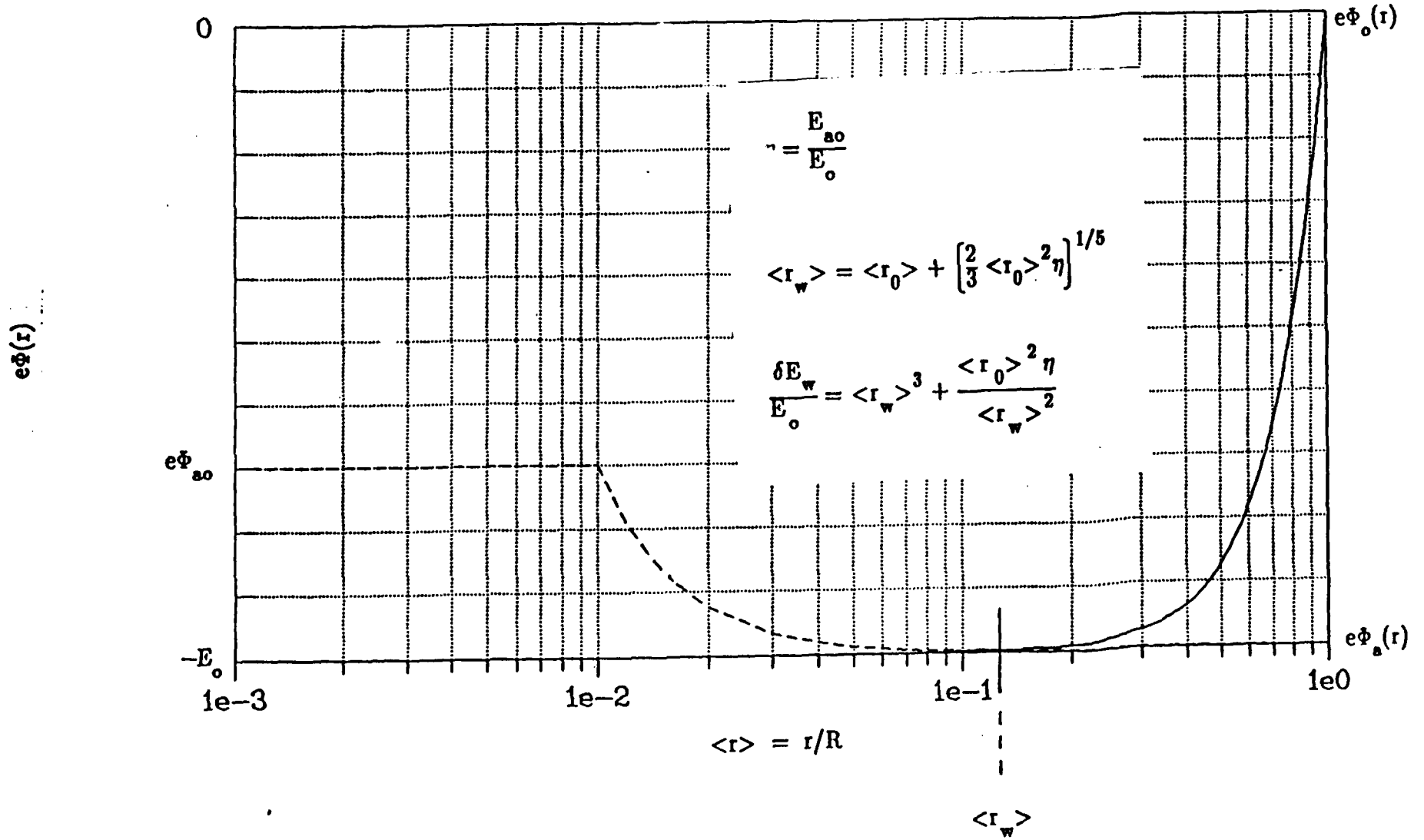

EMC2

Figure 3. Approximate average transit time of electrons, averaged over their initial radial and transverse velocity distributions, through potential well with central virtual anode, as a function of η and $\langle r_o \rangle$.

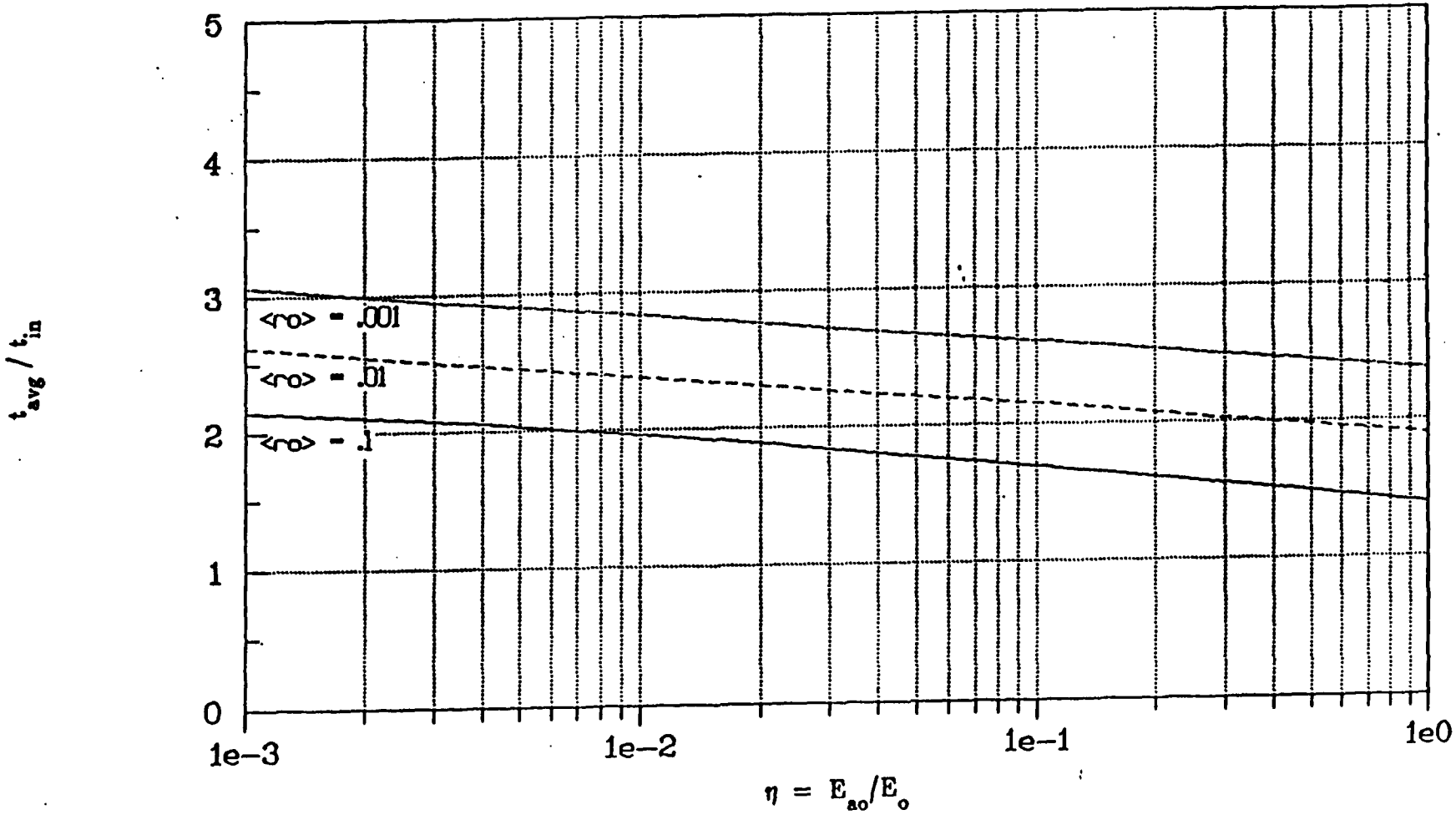

Transit Time Calculations for G_{jo}

$$t_{tot} = \frac{2R}{v_{in}} \left[\frac{\langle r_0 \rangle + \left[\frac{\langle r_w \rangle^2 - \langle r_0 \rangle^2}{2\langle r_0 \rangle} \right]}{\left[\eta + \frac{\delta E_w}{2E_0} \right]^{1/2}} + \frac{2}{\left[1 + \frac{\delta E_w}{2E_0} \right]^{1/2}} \left[\frac{1}{\langle r_w \rangle^{1/2}} - 1 \right] \right]$$

For $\langle r_b \rangle < \langle r_w \rangle$:

$$t_{MR} = \frac{2R}{v_{in}} \left[\frac{\left[\frac{\langle r_w \rangle^2 - \langle r_b \rangle^2}{2\langle r_b \rangle} \right]}{\left[\eta + \frac{\delta E_w}{2E_0} \right]^{1/2}} + \frac{2}{\left[1 + \frac{\delta E_w}{2E_0} \right]^{1/2}} \left[\frac{1}{\langle r_w \rangle^{1/2}} - 1 \right] \right]$$

$$t_{WB} = \frac{2R}{v_{in}} \left[\frac{\langle r_0 \rangle + \left[\frac{\langle r_b \rangle^2 - \langle r_0 \rangle^2}{2\langle r_0 \rangle} \right]}{\left[\eta + \frac{\delta E_w}{2E_0} \right]^{1/2}} \right]$$

For $\langle r_b \rangle > \langle r_w \rangle$:

$$t_{MR} = \frac{2R}{v_{in}} \left[\frac{2}{\left[1 + \frac{\delta E_w}{2E_0} \right]^{1/2}} \left[\frac{1}{\langle r_b \rangle^{1/2}} - 1 \right] \right]$$

$$t_{WB} = \frac{2R}{v_{in}} \left[\frac{\langle r_0 \rangle + \left[\frac{\langle r_w \rangle^2 - \langle r_0 \rangle^2}{2\langle r_0 \rangle} \right]}{\left[\eta + \frac{\delta E_w}{2E_0} \right]^{1/2}} + \frac{2}{\left[1 + \frac{\delta E_w}{2E_0} \right]^{1/2}} \left[\frac{1}{\langle r_w \rangle^{1/2}} - \frac{1}{\langle r_b \rangle^{1/2}} \right] \right]$$

$$\eta = \frac{E_{ao}}{E_o} \qquad \langle r_w \rangle = \langle r_0 \rangle + \left[\frac{2}{m} \langle r_0 \rangle^2 \eta \right]^{1/(m+2)}$$

$$\frac{\delta E_w}{E_o} = \langle r_w \rangle^m + \frac{\langle r_0 \rangle^2 \eta}{\langle r_w \rangle^2}$$

4. Summary of formulae used for total and partial (segmented) electron transit time calculation in virtual anode wells with simple power-law external shape

Mirror/Wiffle Model for G_{jo}

$$G_{jo} = \frac{4}{N} G_{jMRo} \frac{(1-\langle r_b \rangle)\ t_{MR}}{t_{tot}} \qquad r_b < r_x$$

$$G_{jo} = \frac{G_{jMRo}\left[(1-\langle r_b \rangle)\ \frac{4}{N} t_{MR} + (G_{jWB}-1)\langle r_b \rangle t_{WB}\right]}{t_{tot}} \qquad r_b > r_x$$

where:

$$G_{jMRo} = \frac{1}{\langle r_{ad} \rangle^m} \qquad r_b < r_{ad}$$

$$G_{jMRo} = \frac{1}{\langle r_b \rangle^m} \qquad r_b > r_{ad}$$

$$G_{jWB} = \frac{2 r_e Z}{N k_L^2}$$

$$\langle r_b \rangle = (ZW)^{1/(m+2)} \qquad Z = 8\pi n_c r_c^2 \quad \text{and} \quad W = \frac{E_0}{B_0^2 R^2}$$

$$\langle r_x \rangle = \left[\frac{N W k_L^2}{2 r_e}\right]^{1/(m+2)}$$

$$\langle r_{ad} \rangle = \langle r_{ad0} \rangle + k_a(\langle r_b \rangle - \langle r_x \rangle) \qquad \langle r_{ad0} \rangle = \left[\frac{2m^2}{\Gamma_a^2} \frac{W}{r_e}\right]^{1/(m+2)}$$

$$\langle r_g \rangle = \left[\frac{2W}{r_e \langle r \rangle^m}\right]^{\frac{1}{1}} \qquad k_a = \frac{\langle r_k \rangle - \langle r_{ad0} \rangle}{\langle r_k \rangle - \langle r_x \rangle}$$

5. Summary of equations for total electron recirculation ratio, and under mirror reflection (MR) and wiffle-ball (WB) operating modes, and formulae used for critical system radii (gyro, adiabaticity, transition and magnetic pressure balance radii) in simple power-law wells

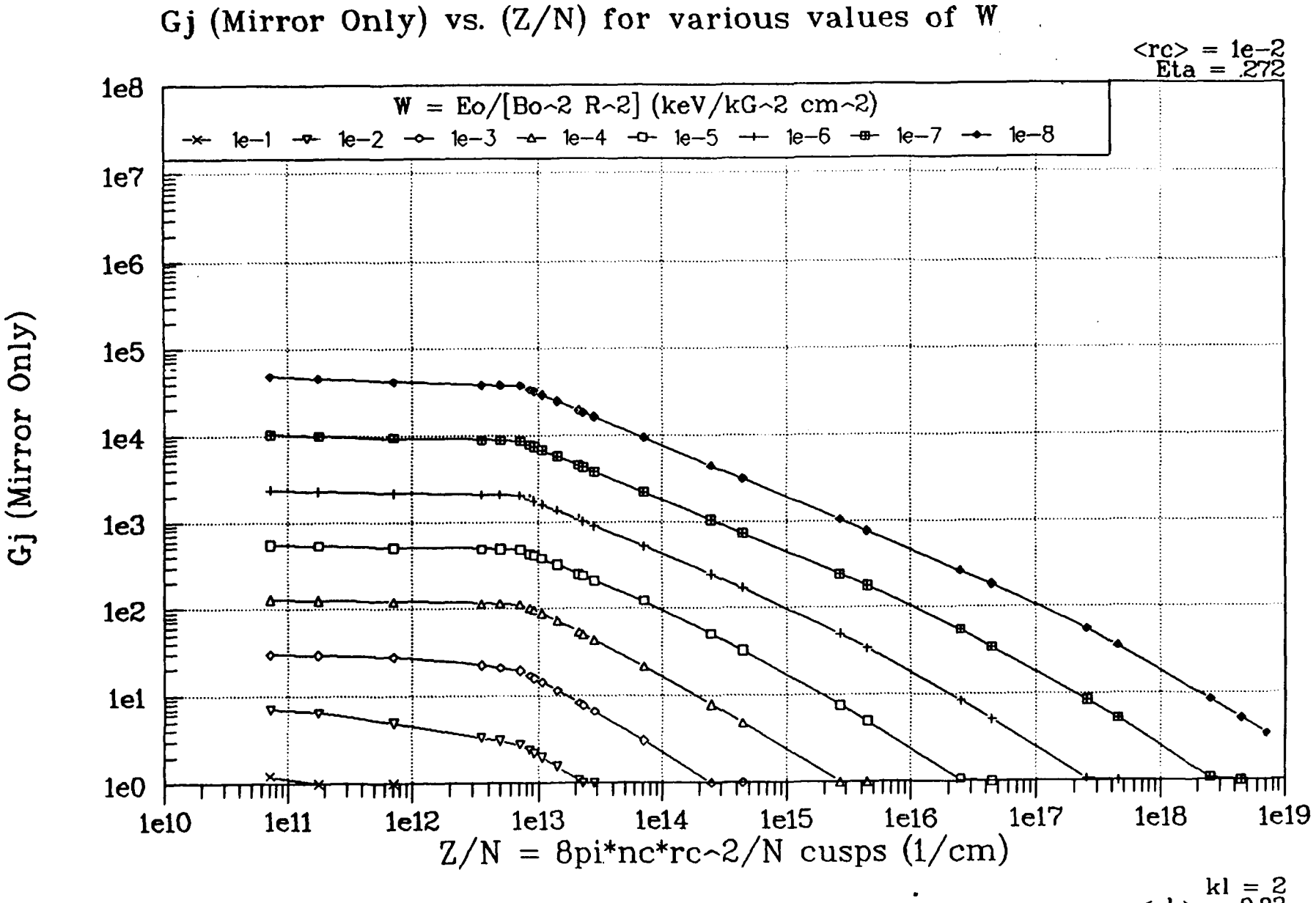

6. Electron recirculation ratio (a) G_{jmr} for MR mode, and (b) G_{jwb} for WB mode operation, as a function of system operating parameter (z), for various values of the system design parameter (w)

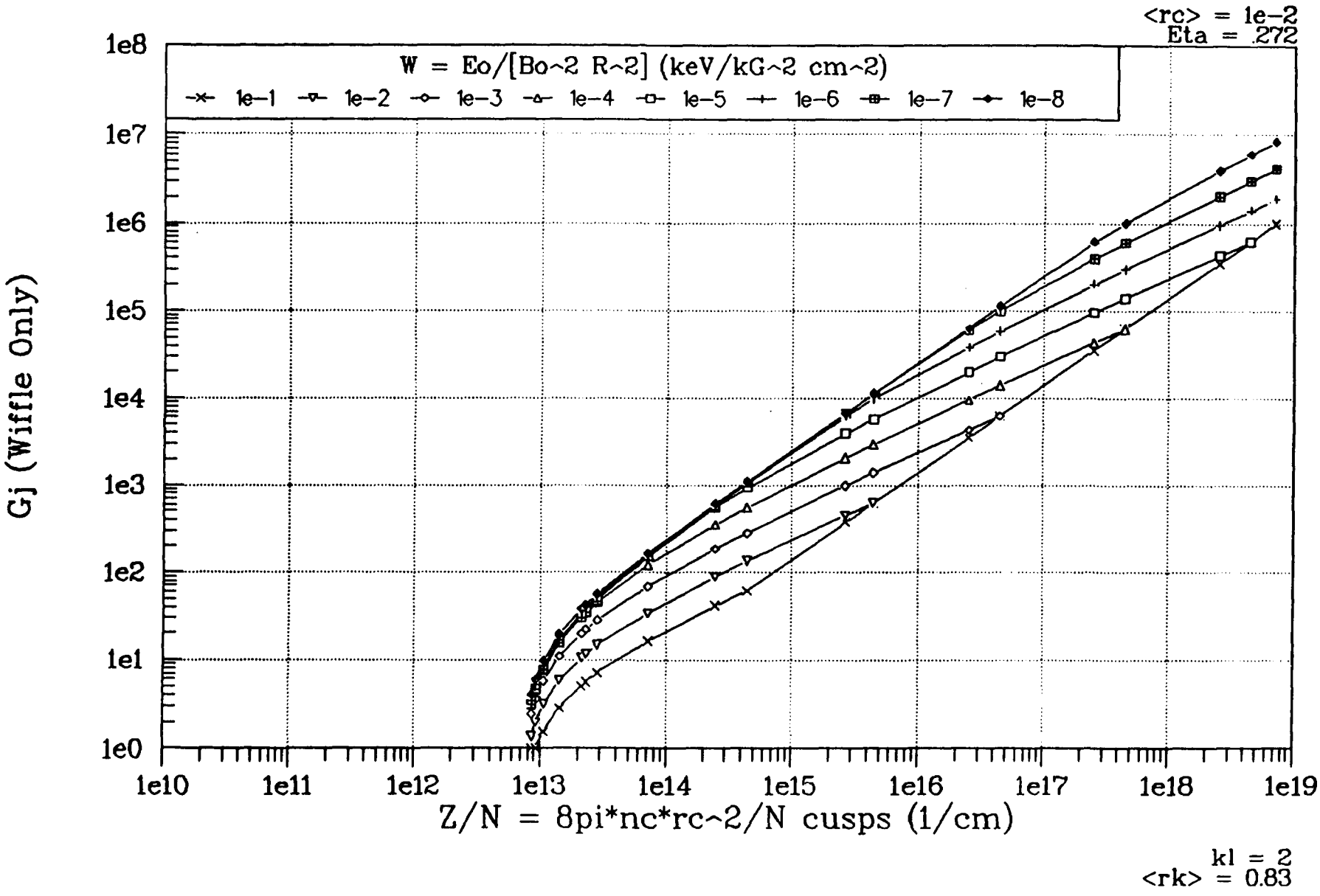

6. Electron recirculation ratio (a) G_{jmr} for MR mode, and (b) G_{jwb} for WB mode operation, as a function of system operating parameter (z), for various values of the system design parameter (w)

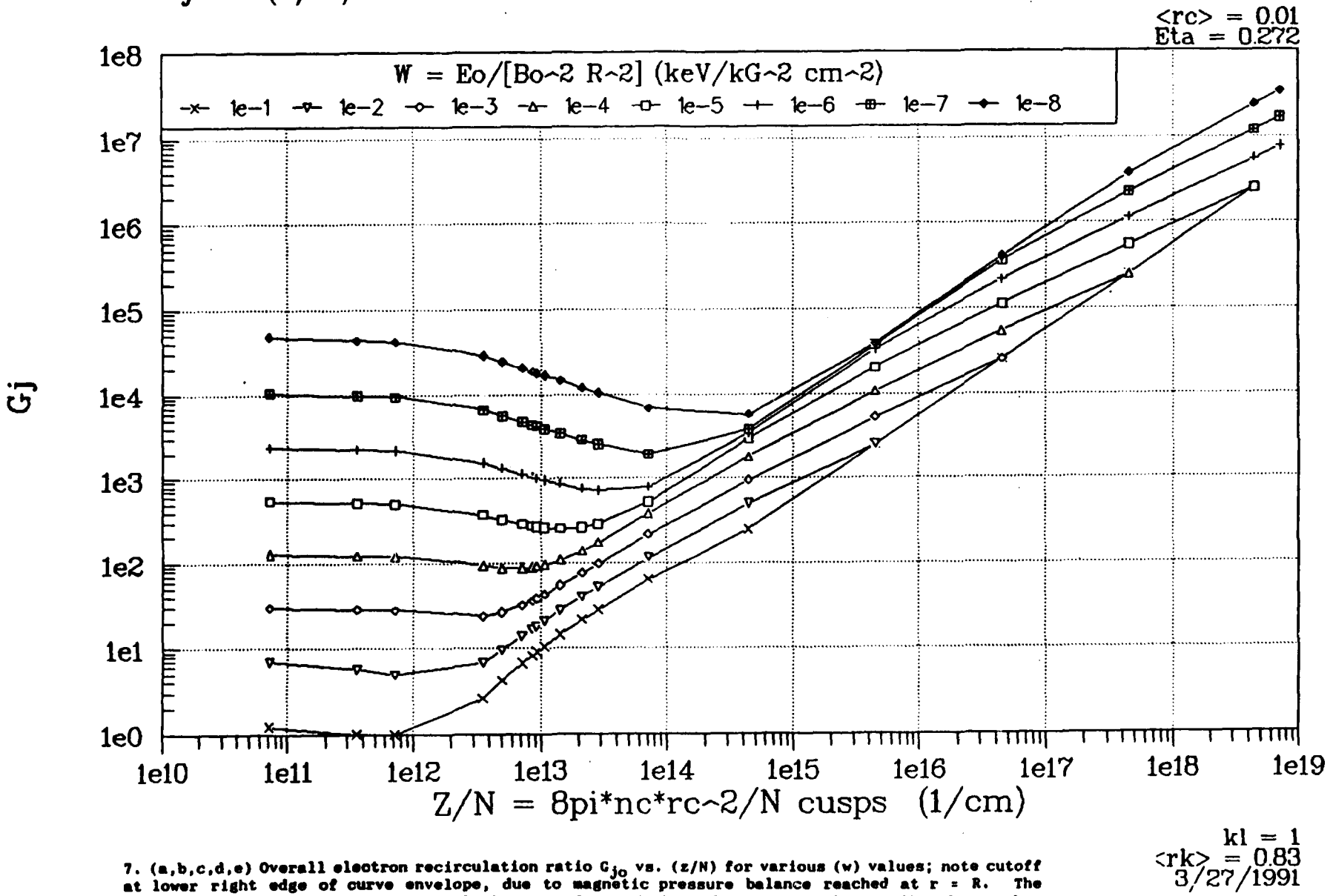

7. (a,b,c,d,e) Overall electron recirculation ratio G_{jo} vs. (z/N) for various (w) values; note cutoff at lower right edge of curve envelope, due to magnetic pressure balance reached at r = R. The different figures are for successively larger values of the effective gyro loss radius factor k_L. Other operating conditions are as marked on the figures

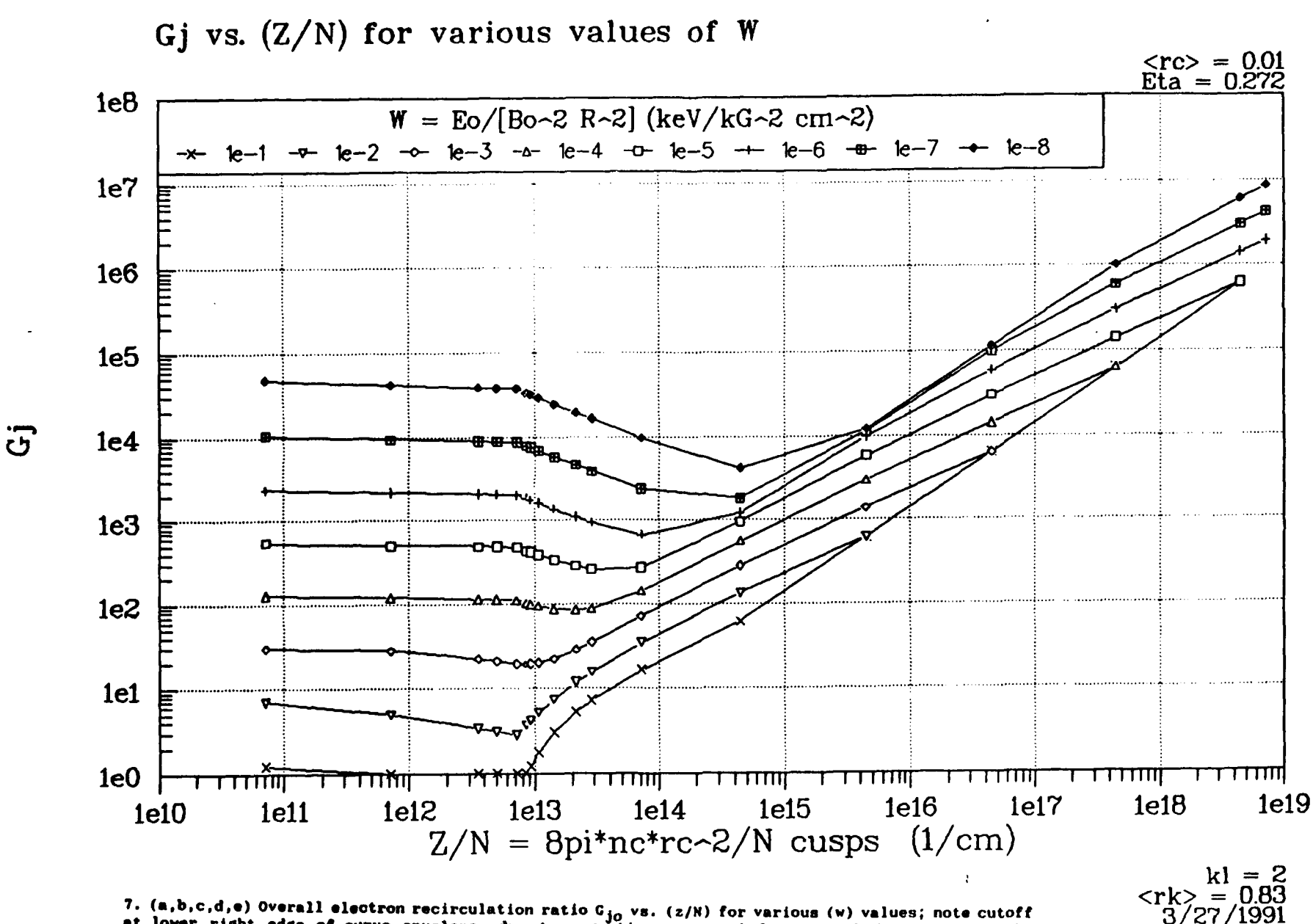

7. (a,b,c,d,e) Overall electron recirculation ratio G_{jo} vs. (z/N) for various (w) values; note cutoff at lower right edge of curve envelope, due to magnetic pressure balance reached at r = R. The different figures are for successively larger values of the effective gyro loss radius factor k_L. Other operating conditions are as marked on the figures

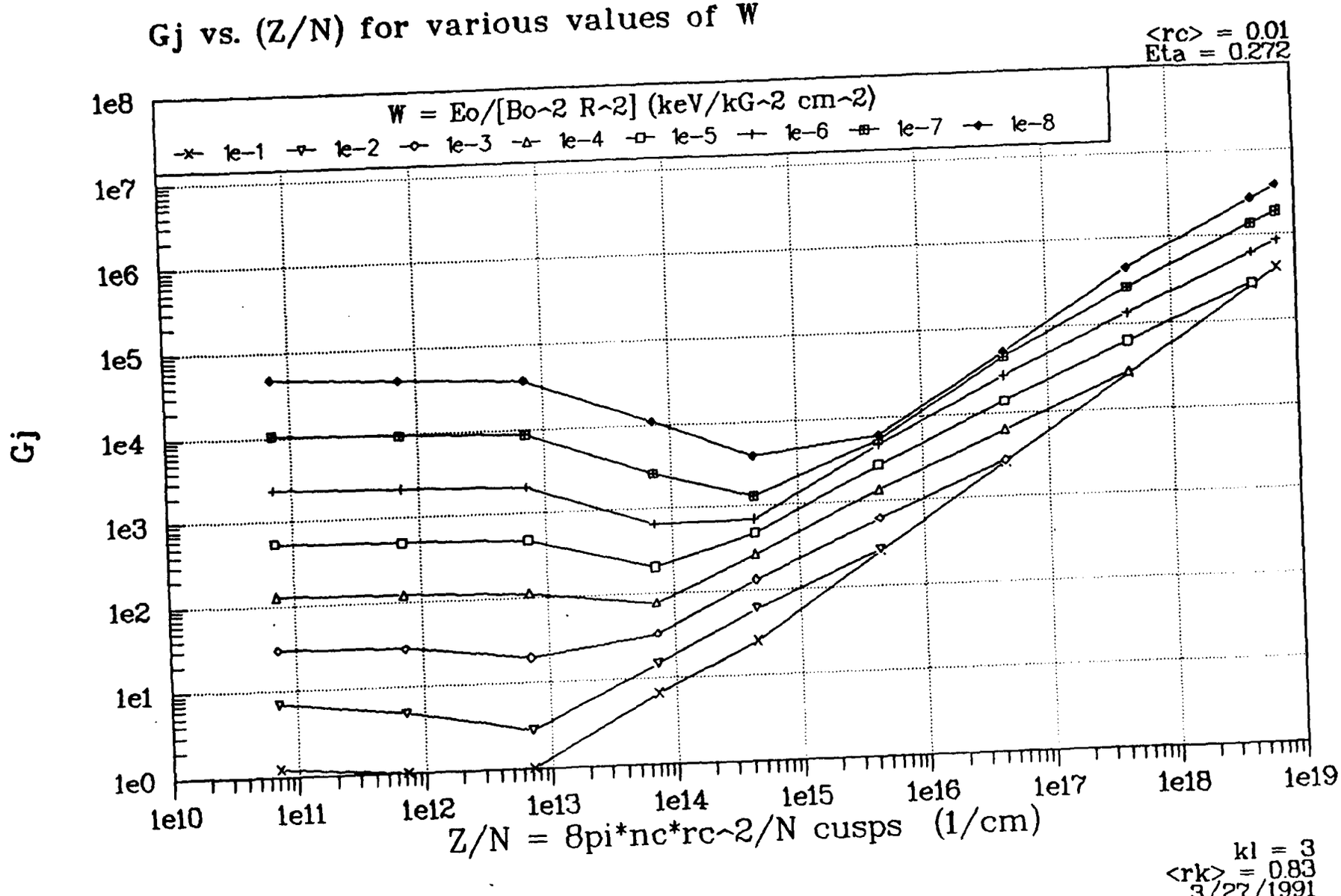

7. (a,b,c,d,e) Overall electron recirculation ratio G_{jo} vs. (z/N) for various (w) values; note cutoff at lower right edge of curve envelope, due to magnetic pressure balance reached at r = R. The different figures are for successively larger values of the effective gyro loss radius factor k_L. Other operating conditions are as marked on the figures

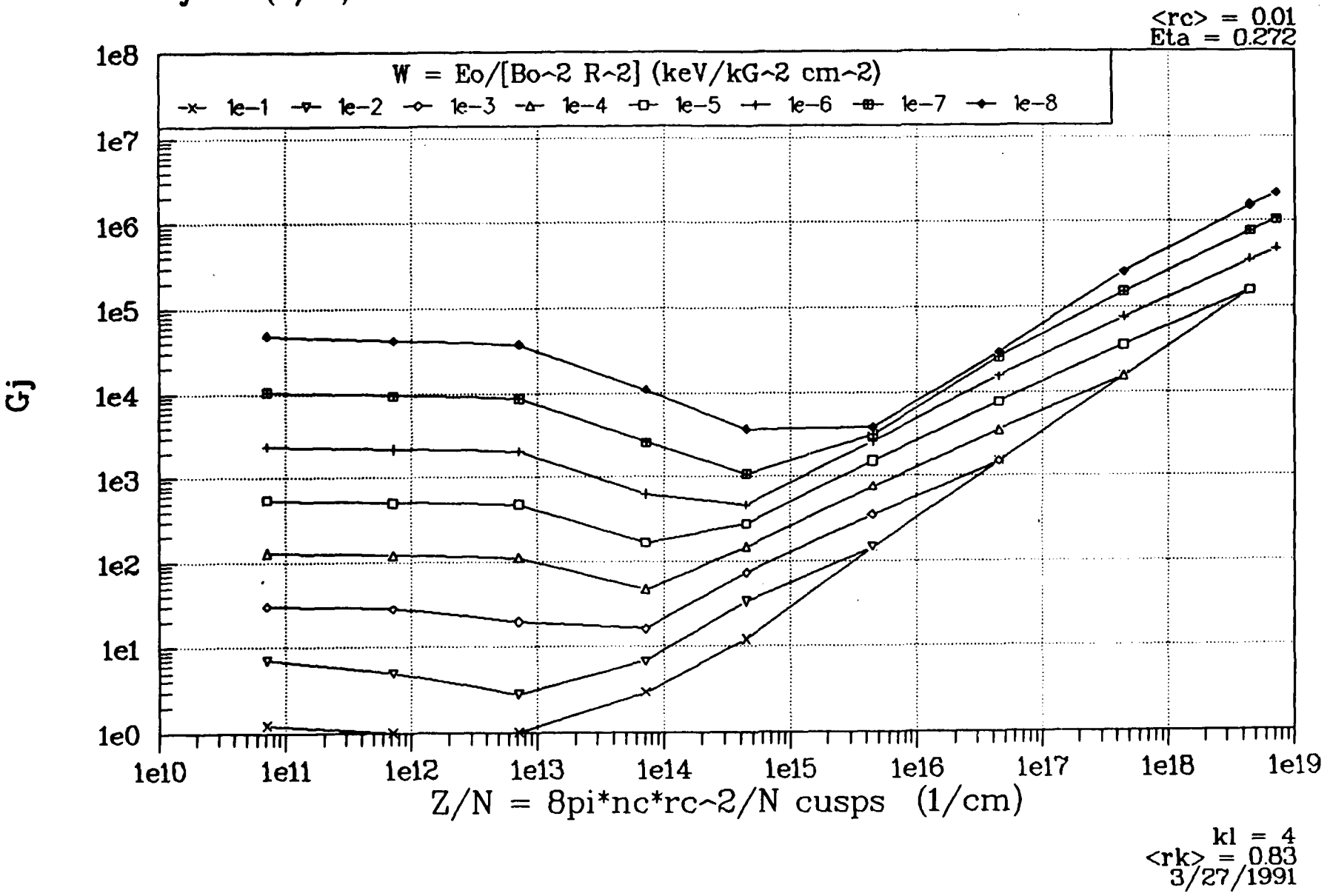

7. (a,b,c,d,e) Overall electron recirculation ratio G_{jo} vs. (z/N) for various (w) values; note cutoff at lower right edge of curve envelope, due to magnetic pressure balance reached at r = R. The different figures are for successively larger values of the effective gyro loss radius factor k_L. Other operating conditions are as marked on the figures

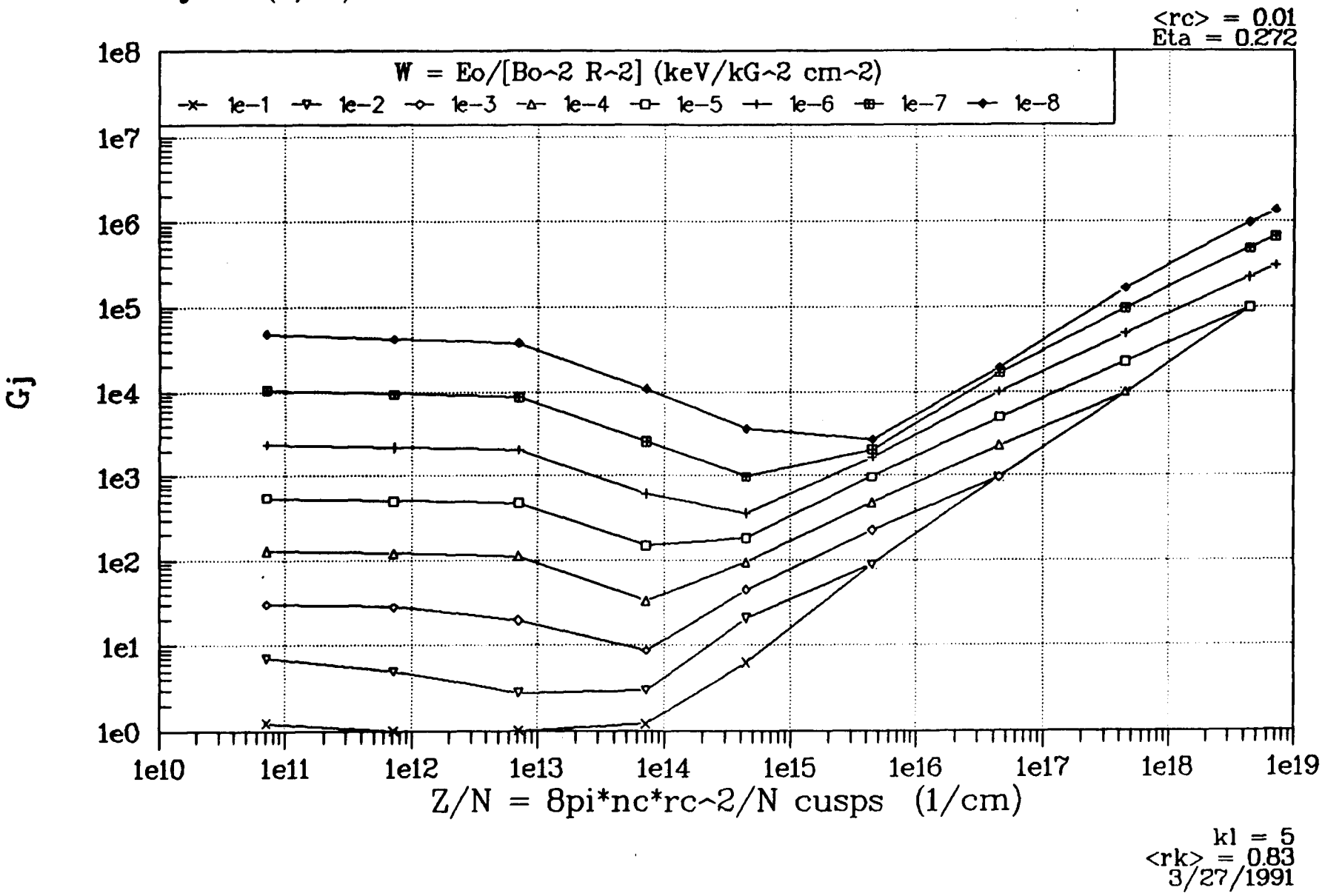

7. (a,b,c,d,e) Overall electron recirculation ratio G_{jo} vs. (z/N) for various (w) values; note cutoff at lower right edge of curve envelope, due to magnetic pressure balance reached at r = R. The different figures are for successively larger values of the effective gyro loss radius factor k_L. Other operating conditions are as marked on the figures

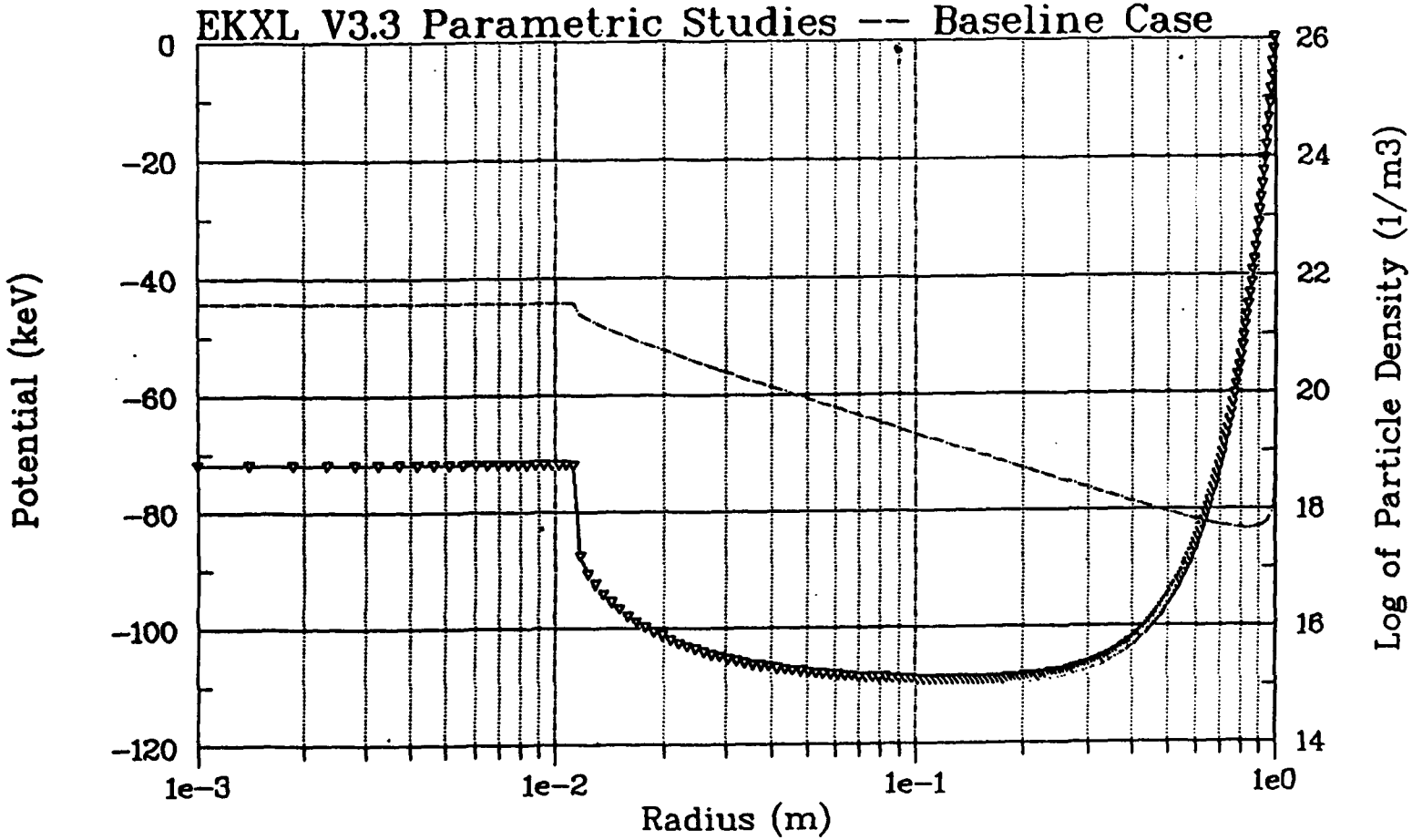

Name	Ig [A]	Einj[eV]	dE[eV]	dEperp[eV]	B and Gi
1) Elec	1.0e03	100.0e03	10.0e03	1.0e03	6.0e03
2) Deut	1.0e02	100.0e00	10.0e00	10.0e00	1.0e03

8. (a) Electric potential, and ion and electron density distributions for a "baseline reactor" case with 1000 A of electrons injected at 100 keV energy into a 1 m radius system with simple power-law field (m = 3) from 6.0 kG at the surface. The unexpanded ion core convergence ratio was taken to be 1E-2, and the virtual anode height was taken to be 0.272. Note expansion of core radius due to ion density compression at virtual anode position

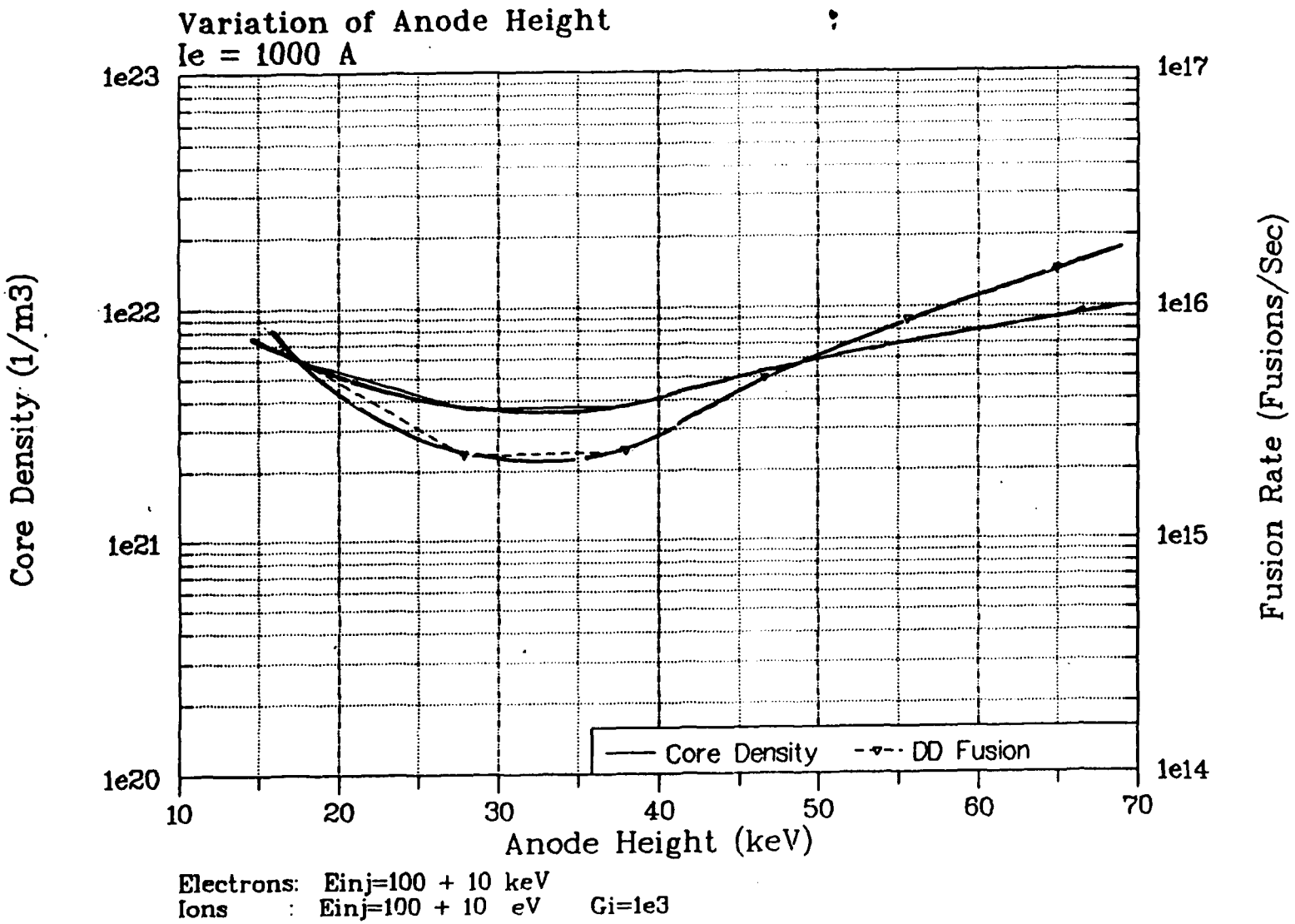

8. (b) Effect of variation of virtual anode (control) height on ion and electron core density and on system fusion rate using DD fuels. Note increasing density and reaction rate at larger anode height, resulting from expansion of central core radius

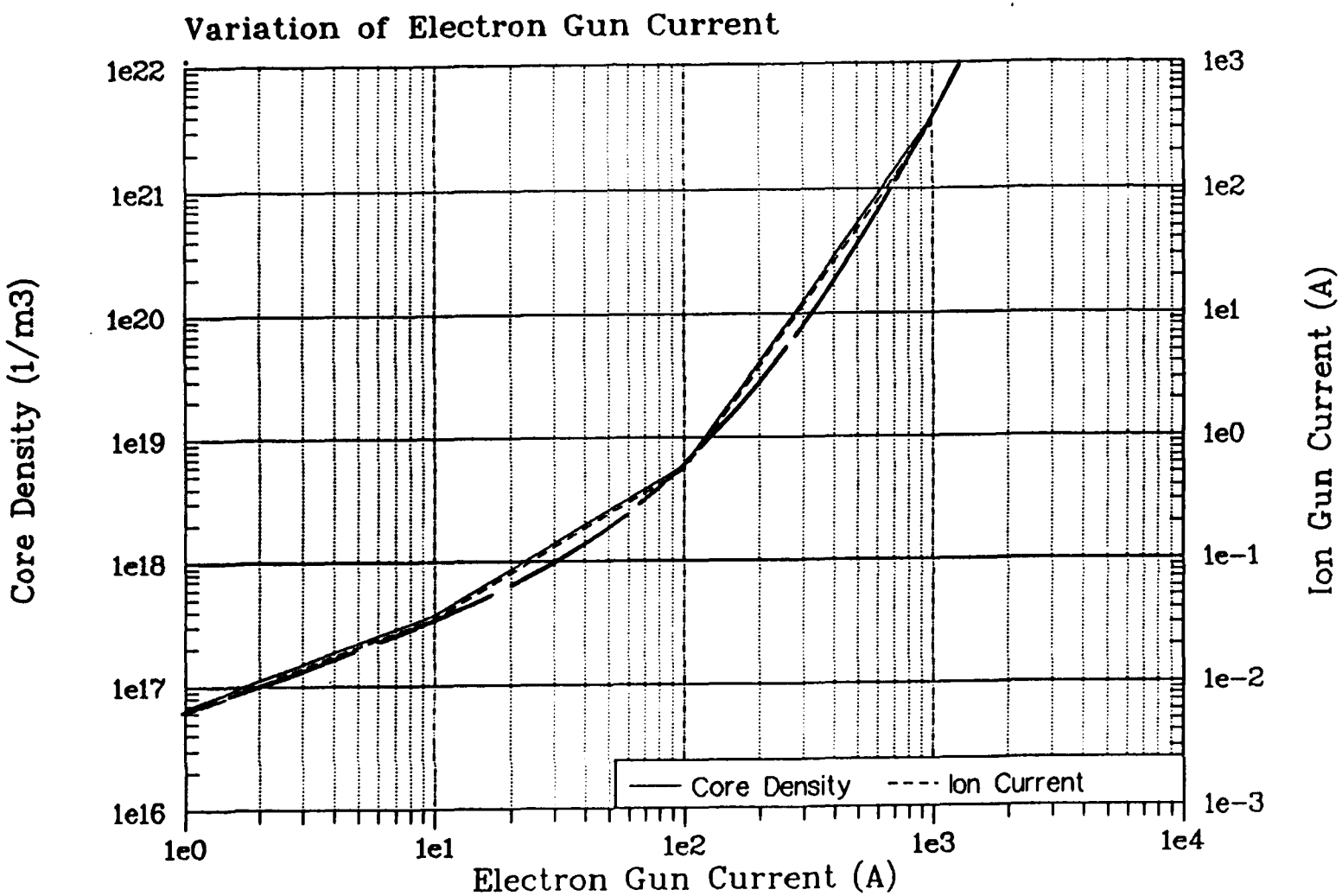

8. (c) Effect of variation of electron gun drive current on required ion current (with G_i = 1000) and on ion and electron core density in baseline case of Figure (8a). Note steep and increasing slope of n_c vs. I_e curve as current is increased above 100 A

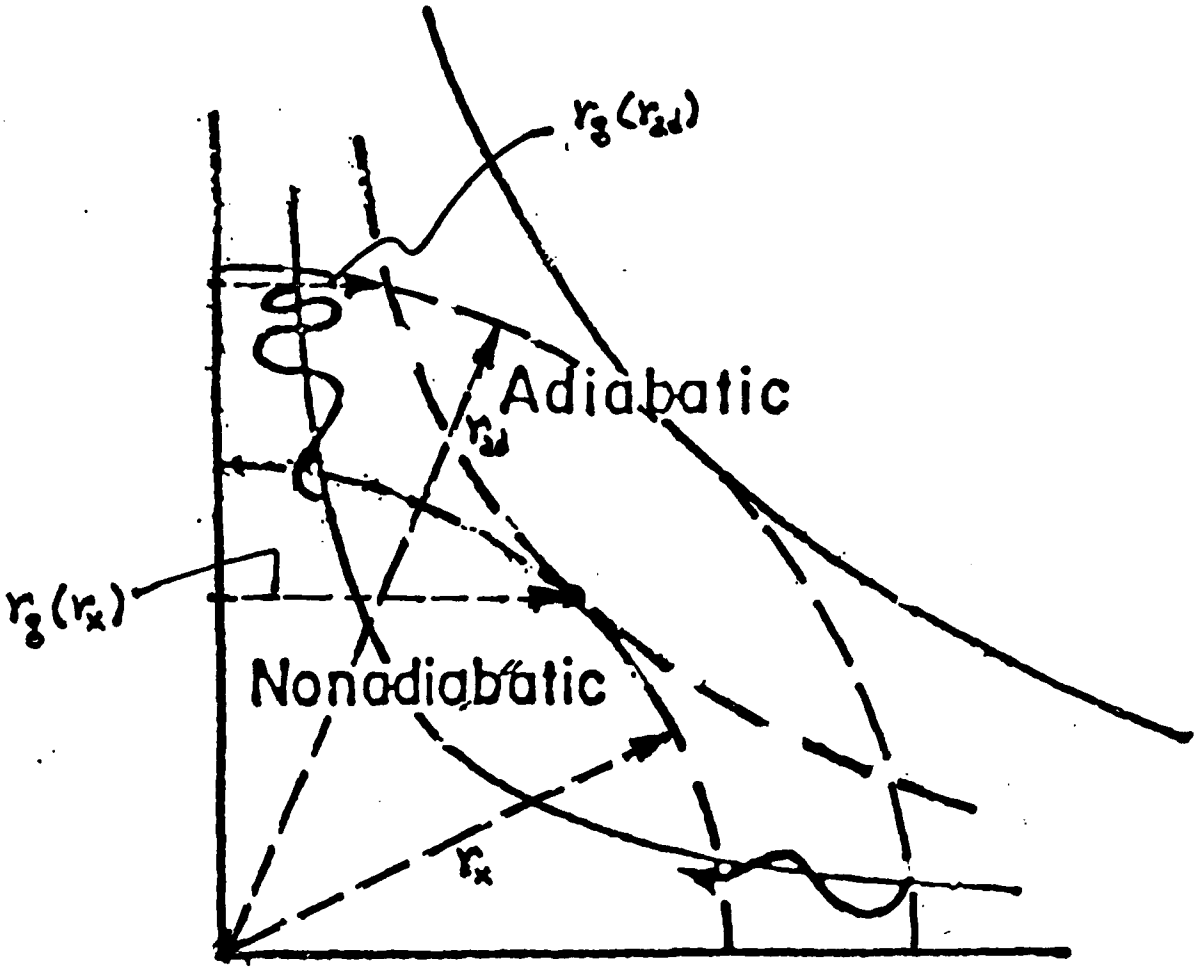

9. Cross section through polar midplane of a biconic "spindle" magnetic cusp system,[16] showing the transition radius r_x and the adiabaticity radius r_{ad}, together with the electron gyro radii at each of these positions in the field. Electrons encountering the cusp "mirrors" at r_x are adiabatically trapped beyond r_{ad}, but reach r_{ad} by traversing the region between the inner solid and middle dashed field envelope lines in the figure, as well as by direct motion from the non-adiabatic region itself.

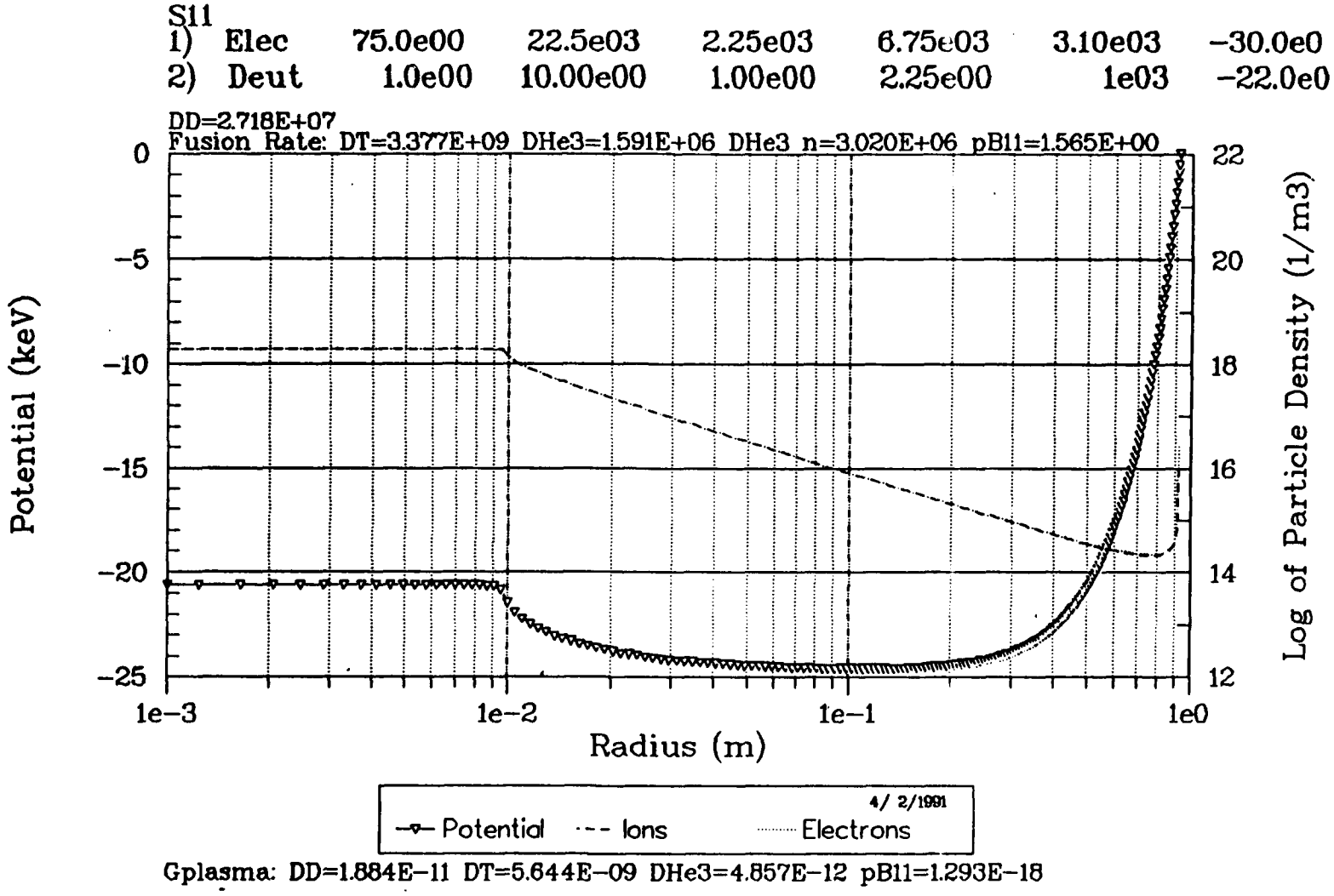

10. Potential and density distributions in SCIF case (a), Table 1, for loss radius factor k_L = 1, showing core density of 2E13/cm^3. Potential to 92 cm edge of system is not shown in this figure

Case1
N=14

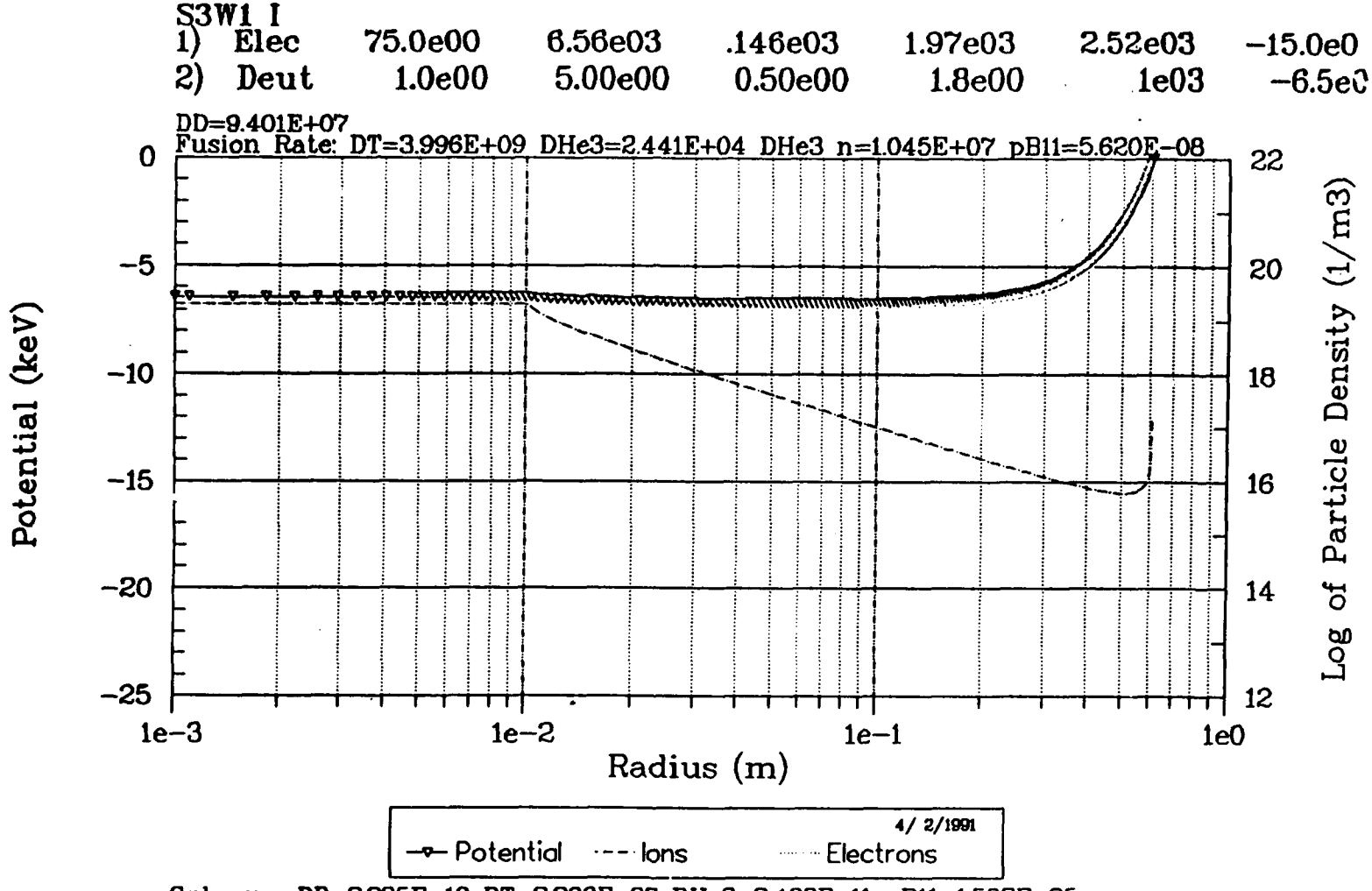

Gplasma: DD=2.235E-10 DT=2.290E-08 DHe3=2.498E-11 pB11=1.592E-25

11. Potential and density distributions in SCIF case (d) of Table 1, for k_L = 1, showing full distributions across complete core; with core density of 1.9E12/cm^3

Case 3
R= 14

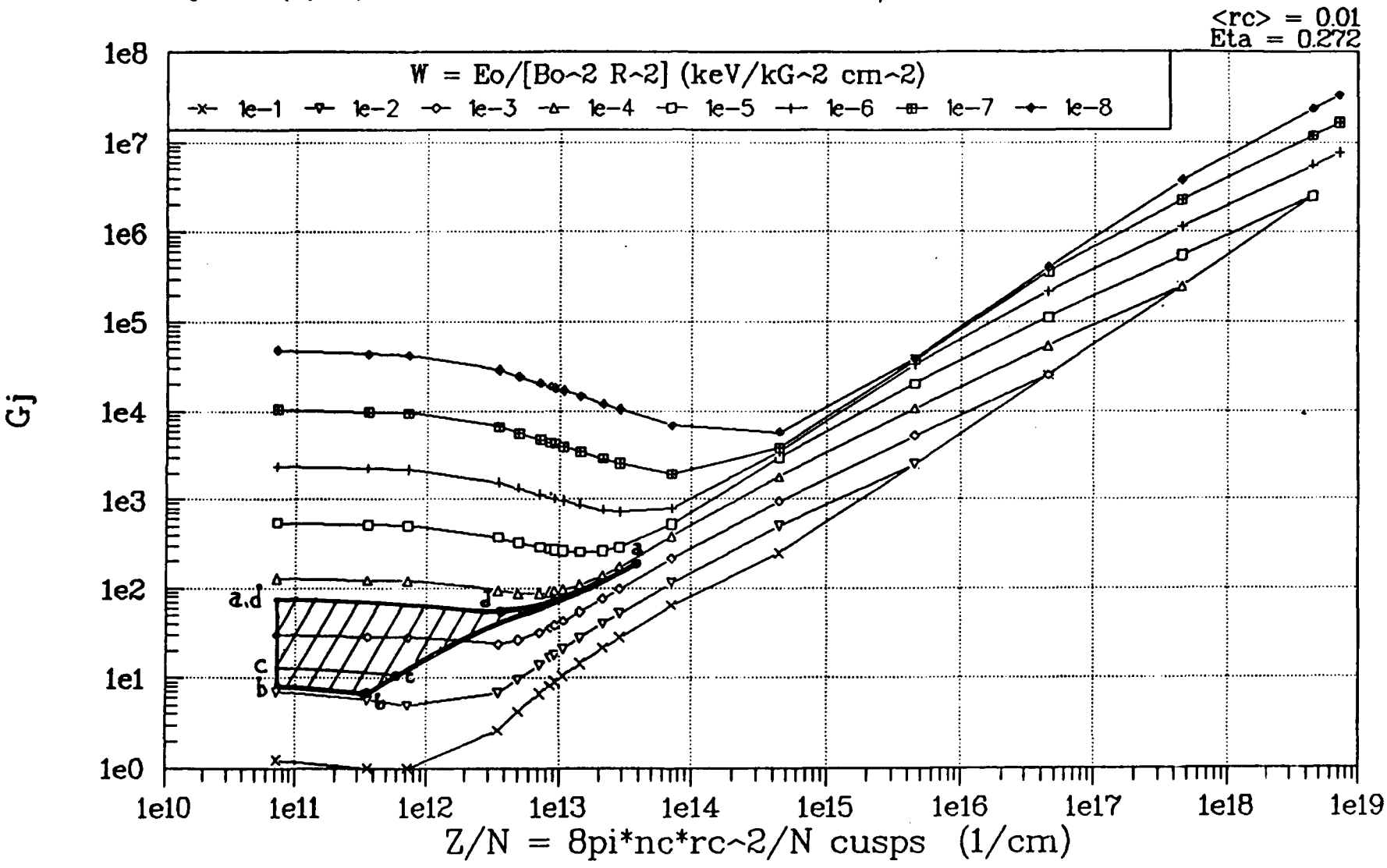

12. Overall system G_j vs. (z/N) for k_L = 1 and k_L = 3 cases, showing the region of parameter space within which the SCIF cases (a-d) of Table 1 can operate. Note that all of these are limited to the far left side of the figures, where operation is entirely in the MR mode, except for the one isolated case (a) extending out into the beginning of the transition region between MR-dominated and WB-dominated mode spaces. Current SCIF systems (cases a-d) seem to be limited to MR mode operation

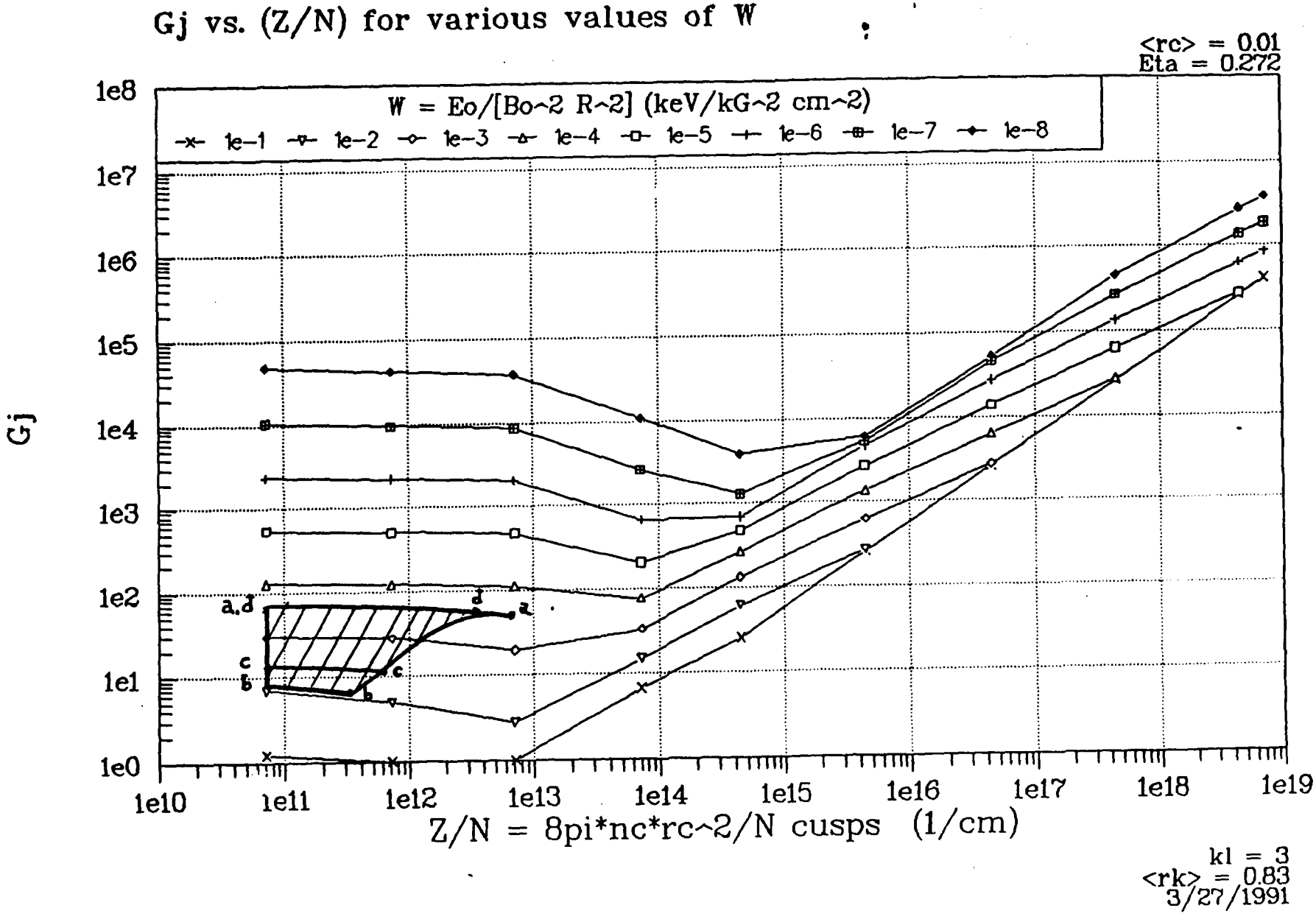

12. Overall system G_j vs. (z/N) for k_L = 1 and k_L = 3 cases, showing the region of parameter space within which the SCIF cases (a-d) of Table 1 can operate. Note that all of these are limited to the far left side of the figures, where operation is entirely in the MR mode, except for the one isolated case (a) extending out into the beginning of the transition region between MR-dominated and WB-dominated mode spaces. Current SCIF systems (cases a-d) seem to be limited to MR mode operation

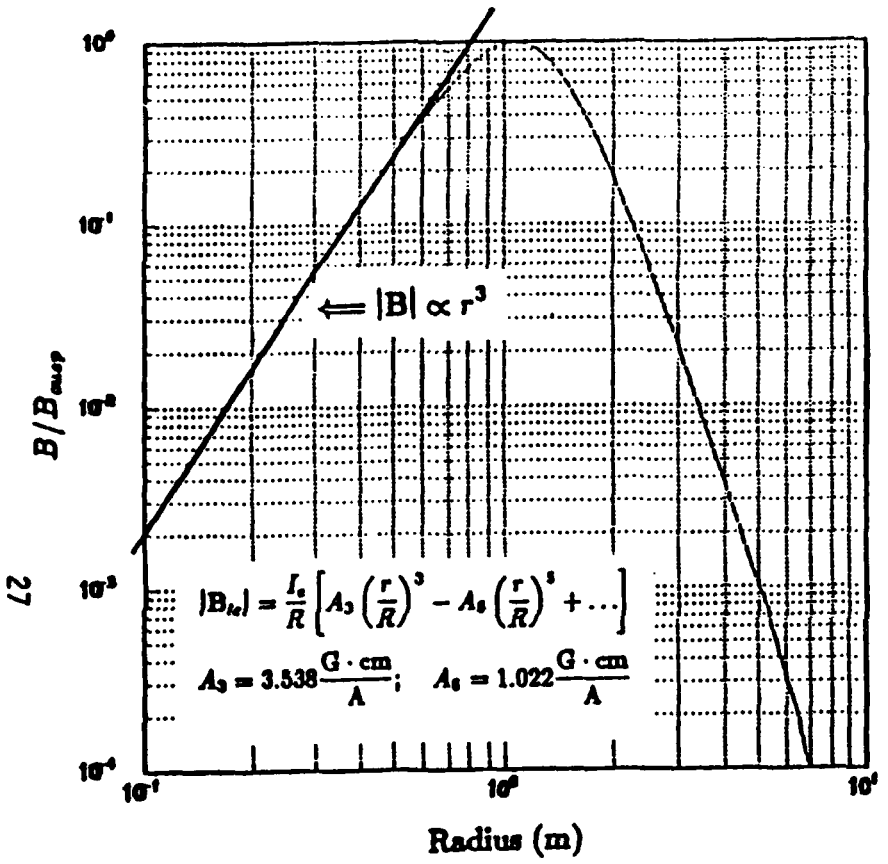

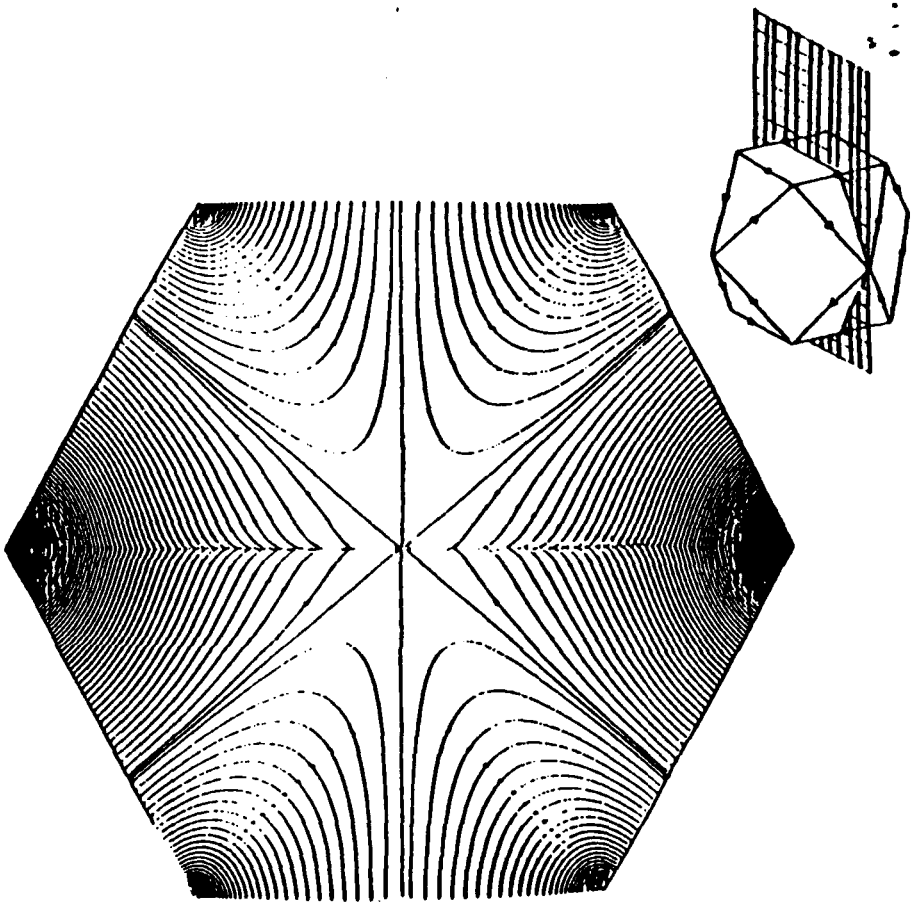

Magnitude of B

Lines of Force

13. Variation of magnetic field in pure linear truncated cube systems, showing "rollover" at edge and field strength 2x higher in interior regions than used in simple power-law model normalized to square face edge field strength